

# Local primordial non-Gaussianity in the relativistic galaxy bispectrum

Roy Maartens<sup>1,2</sup>, Sheean Jolicœur<sup>1</sup>, Obinna Umeh<sup>2</sup>,  
Eline M. De Weerd<sup>3</sup>, Chris Clarkson<sup>3,1</sup>

<sup>1</sup>Department of Physics & Astronomy, University of the Western Cape, Cape Town 7535, South Africa

<sup>2</sup>Institute of Cosmology & Gravitation, University of Portsmouth, Portsmouth PO1 3FX, UK

<sup>3</sup>School of Physics & Astronomy, Queen Mary University of London, London E1 4NS, UK

**Abstract.** Next-generation galaxy and 21cm intensity mapping surveys will rely on a combination of the power spectrum and bispectrum for high-precision measurements of primordial non-Gaussianity. In turn, these measurements will allow us to distinguish between various models of inflation. However, precision observations require theoretical precision at least at the same level. We extend the theoretical understanding of the galaxy bispectrum by incorporating a consistent general relativistic model of galaxy bias at second order, in the presence of local primordial non-Gaussianity. The influence of primordial non-Gaussianity on the bispectrum extends beyond the galaxy bias and the dark matter density, due to redshift-space effects. The standard redshift-space distortions at first and second order produce a well-known primordial non-Gaussian imprint on the bispectrum. Relativistic corrections to redshift-space distortions generate new contributions to this primordial non-Gaussian signal, arising from: (1) a coupling of first-order scale-dependent bias with first-order relativistic observational effects, and (2) linearly evolved non-Gaussianity in the second-order velocity and metric potentials which appear in relativistic observational effects. Our analysis allows for a consistent separation of the relativistic ‘contamination’ from the primordial signal, in order to avoid biasing the measurements by using an incorrect theoretical model. We show that the bias from using a Newtonian analysis of the squeezed bispectrum could be  $\Delta f_{\text{NL}} \sim 5$  for a Stage IV H $\alpha$  survey.

---

## Contents

<b>1</b>	<b>Introduction</b>	<b>2</b>
<b>2</b>	<b>Local primordial non-Gaussianity in the galaxy bias</b>	<b>5</b>
2.1	First-order bias	5
2.2	Second-order bias: Newtonian approximation	7
2.3	Second-order bias: relativistic corrections	8
2.4	Second-order metric and velocity potentials	10
<b>3</b>	<b>Local primordial non-Gaussianity in the relativistic bispectrum</b>	<b>11</b>
3.1	Matter bispectrum	11
3.2	Observed number density	11
3.3	Galaxy bispectrum	13
3.4	Numerical examples	15
<b>4</b>	<b>Conclusions</b>	<b>19</b>
<b>A</b>	<b><math>\beta_I</math> functions in (3.24)</b>	<b>21</b>
<b>B</b>	<b><math>\Upsilon_I</math> functions in (3.26)</b>	<b>26</b>

---

# 1 Introduction

Galaxy number counts are distorted by projection effects that arise from observing on the past lightcone. The dominant perturbative effect on sub-Hubble scales is from redshift-space distortions (RSD) [1, 2], which constitute the standard Newtonian approximation to projection effects. Lensing magnification produces the best-known relativistic correction to RSD [3], but there are further relativistic effects [4–7]. The basic idea is the following. The number of sources above the luminosity threshold,  $dN$ , counted by the observer in a solid angle element about unit direction  $\mathbf{n}$  and in a redshift interval about a central redshift  $z$  is given by

$$dN = N_g dz d\Omega_{\mathbf{n}} = n_g dV. \quad (1.1)$$

The second equality relates the observed quantities to those measured in the rest frame of the source.  $N_g$  is the number that is counted by the observer per redshift per solid angle, while  $n_g$  is the number per proper volume, which is not observed by the observer but is the quantity that would be measured at the source. Similarly,  $dV$  is not the observed volume element but the corresponding proper volume element measured at the source.

Then the observed number density contrast,  $\Delta_g = \delta N_g / \bar{N}_g$ , is related to the proper number density contrast at the source,  $\delta_g = \delta n_g / \bar{n}_g$ , by volume, redshift and luminosity perturbations. At first order in Poisson gauge, the gauge-independent relation (1.1) leads to

$$\begin{aligned} \Delta_g &= \delta_g + \text{RSD} + \text{lensing effect} + \text{other relativistic effects} \\ &= \delta_g - \frac{1}{\mathcal{H}} \mathbf{n} \cdot \nabla (\mathbf{v} \cdot \mathbf{n}) + 2(1 - \mathcal{Q})\kappa + A(\mathbf{v} \cdot \mathbf{n}) + B\Psi + \int d\chi C\Psi' + \int d\chi E\Psi. \end{aligned} \quad (1.2)$$

Here  $\mathcal{H} = d \ln a / d\eta = (\ln a)'$  is the conformal Hubble rate,  $\mathbf{v} = \nabla V$  is the peculiar velocity ( $V$  is not to be confused with the often-used alternative  $v = |\mathbf{v}|$ ),  $\kappa$  is the integrated lensing convergence,  $\mathcal{Q}$  is the magnification bias,  $\chi$  is the comoving line-of-sight distance and the integrals are from source to observer. The perturbed metric is given by

$$a^{-2} ds^2 = -(1 + 2\Phi) d\eta^2 + (1 - 2\Psi) d\mathbf{x}^2, \quad (1.3)$$

and we have assumed  $\Phi = \Psi$ . The time-dependent factors  $A, B, C, E$  in (1.2) correspond respectively to Doppler, Sachs-Wolfe, integrated Sachs-Wolfe and time-delay effects. In Fourier space the Doppler term scales as  $\partial V \propto (\mathcal{H}/k)\delta_m$ , while the remaining terms scale as  $\Psi \propto (\mathcal{H}/k)^2 \delta_m$ . Thus the other relativistic effects are suppressed on sub-Hubble scales, unlike the lensing effect, which scales as  $\partial^2 \Psi \propto \delta_m$ .

The case of 21cm intensity mapping follows from the number count expressions by using the ‘dictionary’ given in [8–10] at first order and in [11–13] at second order.

The physical definition of linear Gaussian galaxy bias is in the joint matter-galaxy rest frame, which corresponds to the comoving gauge (‘C gauge’),<sup>1</sup> so that (omitting luminosity dependence for brevity),

$$\delta_{gC}(a, \mathbf{x}) = b_1(a) \delta_{mC}(a, \mathbf{x}). \quad (1.4)$$

This relation is gauge-independent because C gauge corresponds to the physical rest frame. When transforming to other gauges,  $\delta_g$  is in general no longer proportional to  $\delta_m$  [6, 14, 15]. For example, in the Poisson gauge of (1.2) and (1.3),

$$\delta_g = b_1 \delta_{mC} + (3 - b_e) \mathcal{H} V, \quad b_e = \frac{\partial \ln(a^3 \bar{n}_g)}{\partial \ln a}, \quad (1.5)$$

---

<sup>1</sup>In the  $\Lambda$ CDM model the comoving and synchronous gauges coincide.

where  $b_e$  is known as the evolution bias, which encodes the non-conservation of the background comoving galaxy number density. The velocity potential  $V$  scales as  $\Psi$  by the Euler equation,  $V \propto \Psi \propto (\mathcal{H}/k)^2 \delta_m$ , and therefore the gauge correction  $(3 - b_e)\mathcal{H}V$  is only non-negligible on Hubble scales and may be neglected in a Newtonian approximation.

Local primordial non-Gaussianity (PNG) generates scale-dependent linear bias, with constant parameter  $f_{\text{NL}}$  [16, 17]:

$$b_1(a) \rightarrow b_1(a) + 3 \delta_{\text{crit}} \Omega_{m0} H_0^2 \frac{[b_1(a) - 1]}{D(a)} g_{\text{in}} \frac{f_{\text{NL}}}{T(k)k^2}. \quad (1.6)$$

The threshold density contrast for collapse is usually taken to be  $\delta_{\text{crit}} = 1.686$ , and the growth factor  $D$  is normalised to 1 today ( $a_0 = 1$ ), i.e.  $\delta_m(a, \mathbf{k}) = D(a)\delta_{m0}(\mathbf{k})$ . The growth suppression factor for the potential  $\Psi$  is  $g = D/a$ , which is thus also normalised as  $g_0 = 1$ , with initial value  $g_{\text{in}}$  deep in the matter era, and  $T$  is the transfer function. Note that (1.6) follows the CMB convention for  $f_{\text{NL}}$  [18, 19];  $g_{\text{in}}$  can be removed from (1.6) if  $D$  is normalised as  $D_{\text{in}} = a_{\text{in}}$ . In a  $\Lambda$ CDM model we have the useful relation [20]

$$\frac{g_{\text{in}}}{g} = \frac{3}{5} \left( 1 + \frac{2f}{3\Omega_m} \right), \quad (1.7)$$

where the growth rate of linear matter perturbations,  $f = d \ln D / d \ln a$ , is very well approximated by  $f(a) = \Omega_m(a)^{0.545}$ .

The PNG component of galaxy bias in (1.6) scales as  $H_0^2/k^2$  on ultra-large scales, i.e. above the equality scale,  $k < k_{\text{eq}}$ , where  $T \approx 1$ . It is strongly suppressed on scales  $k \gg k_{\text{eq}}$  by  $T(k)$ . PNG has a similar impact on the power spectrum to the impact of ultra-large-scale relativistic effects. This means that relativistic effects contaminate the primordial signal – leading to biases if a Newtonian approximation is used to model the galaxy power spectrum (see [14, 15, 21]). The relativistic galaxy power spectrum has been used to analyse and predict the capability of future galaxy and intensity mapping surveys to measure the local PNG parameter  $f_{\text{NL}}$ , while avoiding the bias that is inherent in a Newtonian analysis (see e.g. [9, 10, 14, 15, 21–35]).

The tree-level bispectrum requires the number counts in redshift space up to second order. In the Newtonian approximation, the projection effects are the second-order RSD terms (see e.g. [36]). The relativistic corrections to RSD at second-order are extremely complicated, since they involve quadratic couplings of all the first-order terms, as well as introducing new terms that do not enter at first order, such as the transverse peculiar velocity, the lensing deflection angle and the lensing shear [37–41]. There are further relativistic corrections that are not projection effects. Firstly, the Newtonian model of second-order galaxy bias in the comoving frame requires a relativistic correction, unlike the first-order bias (see Section 2). Secondly, and similar to the first-order case, the second-order galaxy bias relation needs relativistic gauge corrections when using non-comoving gauges such as the Poisson gauge. These are second-order extensions of equations like (1.5). In summary, the second-order relativistic corrections to the galaxy bispectrum in the Gaussian case are:

- relativistic projection corrections to the Newtonian RSD [37–41];
- relativistic corrections to the Newtonian bias model in the comoving frame at second order, which were only recently derived [42, 43];
- relativistic gauge corrections to the second-order number density when using non-comoving gauges [37, 38].

As in the case of the power spectrum, local PNG affects the bispectrum on very large scales, which is also where the relativistic effects are strongest. This leads again to a contamination of the primordial signal by relativistic effects, necessitating a relativistic analysis. A Gaussian primordial universe could be mistakenly interpreted as non-Gaussian if a Newtonian model is used for the bispectrum in analysis of the data, as shown by [44–47].

There are important differences between the power spectrum and bispectrum:

- At first order, there is no relativistic correction to the bias model in comoving gauge – the relativistic correction arises at second order [42, 43]. Therefore the tree-level bispectrum contains a relativistic correction to the bias model, but the tree-level power spectrum does not.
- There is no PNG signal in the primordial *matter* power spectrum at tree level, so that the local PNG signal in the tree-level galaxy power spectrum is sourced only by scale-dependent bias.
- By contrast, local PNG in the galaxy bispectrum is sourced by scale-dependent bias, by the primordial matter bispectrum and by RSD at second order (see [36] and Section 2.4 below).
- Second-order relativistic corrections to RSD induce new local PNG effects in the bispectrum, via (1) a coupling of first-order scale-dependent bias to first-order relativistic projection effects, and (2) the linearly evolved PNG in second-order velocity and metric potentials, which appear in relativistic projection effects (absent in the standard Newtonian analysis).

Since local PNG affects the power spectrum and bispectrum differently, a Newtonian analysis could mistakenly identify inconsistencies between the power spectrum and bispectrum  $f_{\text{NL}}$  measurements, which could wrongly lead to an inference of hidden systematics or deviations from general relativity.

PNG in the galaxy bispectrum has been extensively investigated in the Newtonian approximation. Most work has used the Fourier bispectrum, implicitly incorporating a plane-parallel assumption (see e.g. [18, 19, 36, 48–62]) and we follow this approximation. Our previous work [45] included the local (non-integrated) relativistic effects in the Fourier bispectrum for the first time. This was extended by our work [13, 46, 63–68], all in the case of primordial Gaussianity. Here we incorporate local PNG into the relativistic bispectrum. This involves applying the recent results of [42, 43] on relativistic corrections to the second-order galaxy bias model. In addition, we derive the new local PNG terms induced by a coupling of first-order scale-dependent bias and first-order relativistic projection effects and by linearly evolved second-order relativistic projection effects.

The paper is structured as follows. Section 2.4 reviews the relativistic correction to the galaxy bias, including the case of local PNG. In addition, we show how the linearly evolved second-order metric and velocity potentials carry a primordial non-Gaussian signal, which is imprinted in the bispectrum by relativistic projection effects. In Section 3, after presenting the relativistic correction to the matter bispectrum, we discuss the number density contrast in redshift space, which brings into play the relativistic projection effects. We combine the various results to derive the relativistic galaxy bispectrum, including all local PNG effects, and we show examples of the galaxy bispectrum for a Stage IV  $\text{H}\alpha$  spectroscopic survey. We summarise and conclude in Section 4.

### ***Conventions used:***

We assume a flat  $\Lambda$ CDM model, based on general relativity and perturbed up to second order, in which the matter is pressure-free and irrotational on perturbative scales. Generalisations to allow dynamical dark energy and relativistic modified gravity are straightforward, but are not included. For numerical calculations, we use the Planck 2018 best-fit parameters [69]. Perturbed quantities are expanded as  $X + X^{(2)}/2$ , and may be split as  $X_N + X_{GR} + X_{nG}$ , and similarly at second order, where N denotes the Newtonian approximation, GR denotes the relativistic correction and nG denotes the local PNG contribution. GR corrections are highlighted in **magenta**.

Our definition of the metric potentials in (1.3) leads to the first-order Poisson equation

$$\nabla^2 \Psi = +\frac{3}{2}\Omega_m \mathcal{H}^2 \delta_C, \quad (1.8)$$

where  $\Phi = \Psi$  in  $\Lambda$ CDM. Here and in the remainder of the paper, we omit the subscript  $m$  on the matter density contrast for brevity. At second order, the perturbed metric in Poisson gauge is given by

$$a^{-2}ds^2 = -[1 + 2\Psi + \Phi^{(2)}]d\eta^2 + [1 - 2\Psi - \Psi^{(2)}]d\mathbf{x}^2, \quad (1.9)$$

where we neglect vector and tensor modes generated by scalar mode coupling (see [64] for their very small effect on the bispectrum).

## **2 Local primordial non-Gaussianity in the galaxy bias**

Local PNG is defined as a simple form of nonlinearity in the primordial curvature perturbation, which is local in configuration space. In terms of the gravitational potential deep in the matter era, we have

$$-\left[\Psi_{\text{in}}(\mathbf{x}) + \frac{1}{2}\Psi_{\text{in}}^{(2)}(\mathbf{x})\right] = \varphi_{\text{in}}(\mathbf{x}) + f_{\text{NL}}[\varphi_{\text{in}}(\mathbf{x})^2 - \langle \varphi_{\text{in}}^2 \rangle], \quad (2.1)$$

where  $\varphi_{\text{in}}$  is the first-order Gaussian part. The standard definition of  $f_{\text{NL}}$  uses a convention for  $\Psi$  that is different to ours, with a minus on the right of the Poisson equation (1.8). In order to keep the standard sign of  $f_{\text{NL}}$ , we made a sign change on the left of (2.1). ( $f_{\text{NL}}$  in [20, 43, 47] is of opposite sign to the standard sign that we use.)

### **2.1 First-order bias**

In (2.1), the Gaussian part of the potential deep in the matter era (but after decoupling) is related to the linear primordial potential by the transfer function:

$$\varphi_{\text{in}}(\mathbf{k}) = T(k) \varphi_p(\mathbf{k}) \quad \text{for} \quad a_p \ll a_{\text{eq}} \ll a_{\text{in}}. \quad (2.2)$$

Here  $\varphi_p(\mathbf{k}) = -9\Psi(a_p, \mathbf{k})/10$ , where the factor 9/10 ensures conservation of the curvature perturbation on super-Hubble scales. After equality, the potential evolves with the growth suppression factor, so that

$$\varphi(a, \mathbf{k}) = \frac{g(a)}{g_{\text{in}}} \varphi_{\text{in}}(\mathbf{k}) \quad \text{for} \quad a \geq a_{\text{in}} > a_{\text{dec}}. \quad (2.3)$$

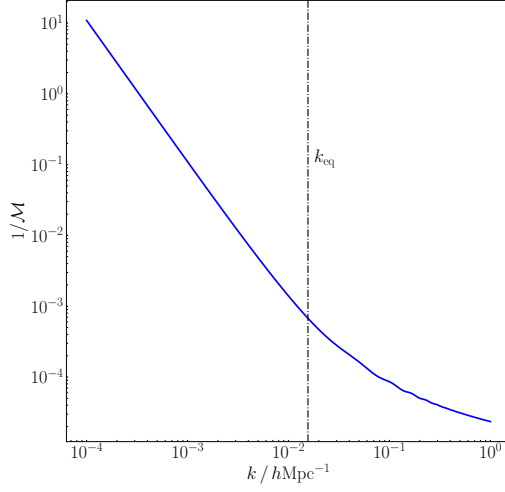


**Figure 1.**  $\mathcal{M}^{-1} = \varphi_p / \delta_C^{(1)}$  at  $z = 1$ .

We relate the late-time matter density contrast to the primordial potential via the Poisson equation (1.8), using (1.7), (2.2) and (2.3):

$$\delta_C(a, \mathbf{k}) = \mathcal{M}(a, k) \varphi_p(\mathbf{k}) \quad \text{where} \quad \mathcal{M}(a, k) = \frac{10}{3\mathcal{H}(a)^2 [3\Omega_m(a) + 2f(a)]} k^2 T(k). \quad (2.4)$$

This relation is illustrated in Fig. 1. The matter and number density contrasts can be written as

$$\delta_C = \delta_{C,N} \quad \text{and} \quad \delta_{gC} = \delta_{gC,N} + \delta_{gC,nG}. \quad (2.5)$$

This follows since there is no GR correction to either contrast and no PNG in the Gaussian matter density contrast:

$$\delta_{C,GR} = 0 = \delta_{gC,GR}, \quad \delta_{C,nG} = 0. \quad (2.6)$$

Then it follows that

$$\delta_{gC} = \delta_{gC,N} + \delta_{gC,nG} = b_{10} \delta_C + b_{01} \varphi_p, \quad (2.7)$$

where the Gaussian and non-Gaussian bias coefficients are

$$b_{10} = b_1, \quad b_{01} = 2f_{NL} \delta_{crit} (b_{10} - 1). \quad (2.8)$$

The relations (2.4)–(2.8) then recover (1.6).

At first order, there is *no* GR correction to the bias relation expressed in the matter-galaxy rest frame. This is no longer true at second order.

The first-order metric potential is Gaussian by (2.1) and has no GR correction by (2.6) and the Poisson equation. From the Euler equation ( $V' + \mathcal{H}V = -\Psi$ ) it follows that the velocity also has no GR and no PNG corrections:

$$\Psi = \Psi_N, \quad V = V_N. \quad (2.9)$$

## 2.2 Second-order bias: Newtonian approximation

At second order, the galaxy bias is physically defined in comoving gauge, but any gauge may be used in general relativity. Standard Newtonian perturbation theory is often given in an Eulerian frame, and so it is useful for comparison to express the bias in a suitable Eulerian frame. We use Poisson gauge here, following [45, 46, 63–67, 70], but with the galaxy and matter density contrasts in total-matter gauge (‘T gauge’). The total-matter gauge is a convenient Eulerian choice for the density contrasts, since it has the same spatial coordinates as the Poisson gauge at first order and the same time-slicing as the comoving gauge at first and second orders [20, 70, 71]. As a result, at first order the total-matter density contrasts coincide with those of the comoving gauge:  $\delta_T = \delta_C$ ,  $\delta_{gT} = \delta_{gC}$ , and we can rewrite (2.7) as

$$\delta_{gT} = \delta_{gT,N} + \delta_{gT,nG} = b_{10} \delta_T + b_{01} \varphi_P = \left(b_{10} + \frac{b_{01}}{\mathcal{M}}\right) \delta_T. \quad (2.10)$$

At second order, the total-matter and Poisson matter density contrasts agree in the Newtonian approximation:  $\delta_{T,N}^{(2)} = \delta_N^{(2)}$ , while the comoving and total-matter Newtonian density contrasts are related via a purely spatial gauge transformation [20, 42, 46, 72]:

$$\delta_{T,N}^{(2)} = \delta_{C,N}^{(2)} + 2\xi^i \partial_i \delta_C, \quad \delta_{gT,N}^{(2)} = \delta_{gC,N}^{(2)} + 2\xi^i \partial_i \delta_{gC}, \quad (2.11)$$

where

$$\xi^i = \partial^i \nabla^{-2} \delta_C = \partial^i \nabla^{-2} \delta_T. \quad (2.12)$$

(The GR parts of the second-order density contrasts in comoving and total-matter gauges are equal; see below.)

For the small scales involved in local clustering of matter density, the Poisson equation at second order has the same Newtonian form as at first order. Then we can extend (2.4) up to second order to define the linearly evolved local PNG part of the density contrast, whose nonlinearity is purely primordial:

$$\delta_{T,nG}^{(2)} = \mathcal{M} \varphi_P^{(2)} = 2f_{NL} \mathcal{M} \varphi_P * \varphi_P, \quad (2.13)$$

where the  $*$  denotes a convolution in Fourier space. This leads to

$$\delta_{T,nG}^{(2)} = 2f_{NL} \mathcal{M}(a, k) \int \frac{d\mathbf{k}'}{(2\pi)^3} \frac{\delta_T(a, \mathbf{k}')}{\mathcal{M}(a, k')} \frac{\delta_T(a, \mathbf{k} - \mathbf{k}')}{\mathcal{M}(a, |\mathbf{k} - \mathbf{k}'|)}. \quad (2.14)$$

In order to include the nonlinearity due to gravitational evolution, we add the standard Newtonian contribution for Gaussian initial conditions to the local PNG part:

$$\begin{aligned} & \delta_{T,N}^{(2)}(a, \mathbf{k}) + \delta_{T,nG}^{(2)}(a, \mathbf{k}) \\ &= \int \frac{d\mathbf{k}'}{(2\pi)^3} \left[ F_2(a, \mathbf{k}', \mathbf{k} - \mathbf{k}') + 2f_{NL} \frac{\mathcal{M}(a, k)}{\mathcal{M}(a, k') \mathcal{M}(a, |\mathbf{k} - \mathbf{k}'|)} \right] \delta_T(a, \mathbf{k}') \delta_T(a, \mathbf{k} - \mathbf{k}'). \end{aligned} \quad (2.15)$$

The standard Newtonian mode-coupling kernel for  $\Lambda$ CDM is [20]:

$$F_2(a, \mathbf{k}_1, \mathbf{k}_2) = 1 + \frac{F(a)}{D(a)^2} + \left(\frac{k_1}{k_2} + \frac{k_2}{k_1}\right) \hat{\mathbf{k}}_1 \cdot \hat{\mathbf{k}}_2 + \left[1 - \frac{F(a)}{D(a)^2}\right] (\hat{\mathbf{k}}_1 \cdot \hat{\mathbf{k}}_2)^2, \quad (2.16)$$

where  $F$  is the second-order growth factor. The Einstein–de Sitter relation  $F/D^2 = 3/7$  is a very good approximation in  $\Lambda$ CDM. We use this approximation, in which  $F_2$  is effectively time independent.



At second order, the standard Newtonian bias model, including tidal bias in the Gaussian part and all local PNG contributions, is given by (see [19] for a comprehensive treatment):

$$\begin{aligned} \delta_{gT,N}^{(2)} + \delta_{gT,nG}^{(2)} = & b_{10} \delta_{T,N}^{(2)} + b_{20} (\delta_T)^2 + b_s s^2 \\ & + b_{10} \delta_{T,nG}^{(2)} + b_{11} \delta_T \varphi_p + b_n \xi^i \partial_i \varphi_p + b_{02} (\varphi_p)^2. \end{aligned} \quad (2.17)$$

The (Eulerian) bias parameters in the case of Gaussian initial conditions are in the first line on the right-hand side: the linear and quadratic biases,  $b_{10}$  and  $b_{20}$ , and the tidal bias  $b_s$ , where

$$s^2 = s_{ij} s^{ij}, \quad s_{ij} = \left( \partial_i \partial_j - \frac{1}{3} \delta_{ij} \nabla^2 \right) \nabla^{-2} \delta_T. \quad (2.18)$$

The second line of (2.17) contains the local PNG contribution, with three new bias parameters  $b_{11}, b_n, b_{02}$ . The first term is the primordial dark matter contribution, from (2.15); note that  $\tilde{\delta}_{T,N}^{(2)}$  is proportional to  $f_{NL}$ . The  $b_{11}, b_n$  terms scale as  $(\mathcal{H}^2/k^2) (\delta_T)^2$ , while the  $b_{02}$  term is  $\mathcal{O}(\mathcal{H}^4/k^4)$ . The new bias parameters vanish when  $f_{NL} = 0$ ; in the presence of local PNG, they are given by [19, 43, 53]:

$$b_{11} = 4f_{NL} \left[ \delta_{\text{crit}} b_{20} + \left( \frac{13}{21} \delta_{\text{crit}} - 1 \right) (b_{10} - 1) + 1 \right], \quad (2.19)$$

$$b_n = 4f_{NL} \left[ \delta_{\text{crit}} (1 - b_{10}) + 1 \right], \quad (2.20)$$

$$b_{02} = 4f_{NL}^2 \delta_{\text{crit}} \left[ \delta_{\text{crit}} b_{20} - 2 \left( \frac{4}{21} \delta_{\text{crit}} + 1 \right) (b_{10} - 1) \right]. \quad (2.21)$$

Note that the expressions for the bias coefficients in (2.19)–(2.21), as well as for  $b_{01}$  in (2.8), are based on a universal halo mass function.

### 2.3 Second-order bias: relativistic corrections

The relativistic second-order galaxy bias model has been derived in [42] (Gaussian case) and [43] (with local PNG). The key feature to bear in mind is the following:

*GR corrections in the galaxy number density contrast  $\delta_{gT}^{(2)}$  do not change the galaxy bias terms in (2.17), which contain all the local PNG effects.*

This separation between GR effects and local PNG in the number density can be understood as follows.

- The intrinsic nonlinearity of GR modulates the galaxy number density via large-scale modes. However, this does not affect small-scale clustering: GR effects do *not* modulate the variance of small-scale density modes [47, 73, 74].
- By contrast, local PNG imprints a primordial long-short coupling that induces a long-mode modulation of the variance and thus changes the galaxy bias.

As a consequence, we expect that relativistic corrections to the bias relation should be independent of non-Gaussianity and apply only on ultra-large scales (for a different view, see [75]). These two features are consistent with the behaviour of (2.17) under change of gauge:

The Newtonian bias relation (2.17) is gauge-independent only on small scales. Relativistic corrections to (2.17) are needed to enforce gauge-independence of the bias relation on ultra-large scales.

As shown in [42, 43], gauge-independence requires the addition to (2.17) of the relativistic part of the second-order matter density contrast. The relativistic modes are super-Hubble at equality and arise from nonlinear GR corrections to the Newtonian Poisson equation [20, 70, 71, 76]:

$$\delta_{\text{C,GR}}^{(2)} = \delta_{\text{T,GR}}^{(2)} = \frac{20}{3} \delta_{\text{T}} \hat{\varphi}_{\text{in}} - \frac{5}{3} \xi^i \partial_i \hat{\varphi}_{\text{in}} \equiv \delta_{g\text{T,GR}}^{(2)}. \quad (2.22)$$

Here  $\hat{\varphi}_{\text{in}}$  is the ultra-large scale potential deep in the matter era,

$$\hat{\varphi}_{\text{in}}(\mathbf{k}) = \varphi_{\text{in}}(\mathbf{k} \mid k < k_{\text{eq}}). \quad (2.23)$$

When we relate  $\hat{\varphi}_{\text{in}}$  to the density contrast today, via (2.2) and (2.4), we need to impose  $T = 1$  on the transfer function, by (2.23).

The relativistic second-order galaxy bias model of [43] can be written in T-gauge as

$$\delta_{g\text{T}}^{(2)} = \delta_{g\text{T,N}}^{(2)} + \delta_{g\text{T,nG}}^{(2)} + \delta_{g\text{T,GR}}^{(2)}, \quad (2.24)$$

where

$$\delta_{g\text{T,N}}^{(2)} = b_{10} \delta_{\text{T,N}}^{(2)} + b_{20} (\delta_{\text{T}})^2 + b_s s^2, \quad (2.25)$$

$$\delta_{g\text{T,nG}}^{(2)} = b_{10} \delta_{\text{T,nG}}^{(2)} + b_{11} \delta_{\text{T}} \varphi_{\text{p}} + b_n \xi^i \partial_i \varphi_{\text{p}} + b_{02} (\varphi_{\text{p}})^2, \quad (2.26)$$

$$\delta_{g\text{T,GR}}^{(2)} = \frac{20}{3} \delta_{\text{T}} \hat{\varphi}_{\text{in}} - \frac{5}{3} \xi^i \partial_i \hat{\varphi}_{\text{in}}. \quad (2.27)$$

Here (2.25) and (2.26) recover the Newtonian relation (2.17).

Both the local PNG and GR terms scale as  $(\mathcal{H}^2/k^2) (\delta_{\text{T}})^2$ , so that the GR correction *cannot* be neglected. Although they are of the same order of magnitude, there is a key distinction between them: local PNG induces a short-long mode coupling, and thus affects the primordial potential  $\varphi_{\text{p}}$  on small scales, while the GR corrections affect only the ultra-large-scale primordial modes. In the absence of local PNG, i.e. for  $f_{\text{NL}} = 0$ , the GR terms survive and constitute the relativistic bias correction in the case of Gaussian initial conditions, as derived in [42].

Finally, we transform (2.10) and (2.24) to Poisson gauge:

$$\delta_g = \delta_{g\text{T}} + (3 - b_e) \mathcal{H} V, \quad (2.28)$$

$$\begin{aligned} \delta_g^{(2)} = & \delta_{g\text{T}}^{(2)} + (3 - b_e) \mathcal{H} V^{(2)} + \left[ (b_e - 3) \mathcal{H}' + (b_e - 3)(b_e - 4) \mathcal{H}^2 + b_e' \mathcal{H} \right] (V)^2 \\ & + 2(3 - b_e) \mathcal{H} V \delta_{g\text{T}} - 2V \delta_{g\text{T}}' + 2(3 - b_e) \mathcal{H} V \Psi, \end{aligned} \quad (2.29)$$

where the GR corrections in magenta scale as  $(\mathcal{H}^2/k^2) \delta_{\text{T}}$  at first order, and as  $(\mathcal{H}^2/k^2) (\delta_{\text{T}})^2$  or  $(\mathcal{H}^4/k^4) (\delta_{\text{T}})^2$  at second order. For (2.29) we followed [38, 46, 67], but we significantly simplified their expressions, using the first-order Euler equation  $V' + \mathcal{H} V = -\Psi$  and the relation

$$V = -\frac{2f}{3\Omega_m \mathcal{H}} \Psi, \quad (2.30)$$

which follows from the continuity equation,  $\delta_{\text{T}}' = -\nabla^2 V$ , and the Poisson equation. We also included the evolution bias terms that are omitted in [43].

## 2.4 Second-order metric and velocity potentials

At second order, the number density contrast has a GR correction in addition to a PNG correction, as shown in (2.24). Unlike the first-order case, the metric and velocity potentials at second order also have nonzero GR and PNG corrections:

$$\Psi^{(2)} = \Psi_N^{(2)} + \Psi_{\text{GR}}^{(2)} + \Psi_{\text{nG}}^{(2)}, \quad (2.31)$$

$$\Phi^{(2)} = \Psi_N^{(2)} + \Phi_{\text{GR}}^{(2)} + \Psi_{\text{nG}}^{(2)}, \quad (2.32)$$

$$V^{(2)} = V_N^{(2)} + V_{\text{GR}}^{(2)} + V_{\text{nG}}^{(2)}, \quad (2.33)$$

where we note that

$$\Phi_N^{(2)} = \Psi_N^{(2)} \quad \text{and} \quad \Phi_{\text{nG}}^{(2)} = \Psi_{\text{nG}}^{(2)}. \quad (2.34)$$

The GR corrections are derived in [20] (which only considers modes  $k < k_{\text{eq}}$ ). Here we derive the PNG contributions, which include modes  $k > k_{\text{eq}}$ .

The PNG corrections to metric and velocity potentials are linearly evolved, i.e., their nonlinearity is purely primordial, the same as in the case of the density contrast. They follow from constraint and energy conservation equations applied to the linearly evolved PNG part of the matter density contrast,  $\delta_{\text{T,nG}}^{(2)}$ . As we argued in deriving (2.14),  $\delta_{\text{T,nG}}^{(2)}$  obeys the linear Newtonian Poisson equation. The same applies to the linearly evolved  $\Psi_{\text{nG}}^{(2)}$ . From the Newtonian Poisson equation we find that

$$\begin{aligned} \Psi_{\text{nG}}^{(2)}(a, \mathbf{k}) &= -\frac{3\Omega_m(a)\mathcal{H}(a)^2}{2k^2} \delta_{\text{T,nG}}^{(2)}(a, \mathbf{k}) \\ &= -\frac{10}{3}f_{\text{NL}} \left[ 1 + \frac{2f(a)}{3\Omega_m(a)} \right]^{-1} T(k) (\varphi_{\text{p}} * \varphi_{\text{p}})(\mathbf{k}), \end{aligned} \quad (2.35)$$

where we used (2.4) and (2.14).

By (2.35),  $\Psi_{\text{nG}}^{(2)}$  grows as  $(1 + 2f/3\Omega_m)^{-1}$ , and thus

$$\Psi_{\text{nG}}^{(2)'} = -\frac{2f}{(3\Omega_m + 2f)} \left( \frac{f'}{f} + \mathcal{H} + 2\frac{\mathcal{H}'}{\mathcal{H}} \right) \Psi_{\text{nG}}^{(2)}. \quad (2.36)$$

The first-order linear equation (2.30), based on energy conservation and the Poisson equation, extends to second order for the linearly evolved PNG parts of the velocity and the potential. This determines the PNG part of the velocity:

$$V_{\text{nG}}^{(2)} = -\frac{2f}{3\Omega_m \mathcal{H}} \Psi_{\text{nG}}^{(2)}. \quad (2.37)$$

The linearly evolved PNG part of the second-order RSD term then follows as

$$\partial_{\parallel}^2 V_{\text{nG}}^{(2)}(a, \mathbf{k}) = -2f_{\text{NL}} \mathcal{H}(a)f(a)\mu^2 \mathcal{M}(a, k) (\varphi_{\text{p}} * \varphi_{\text{p}})(\mathbf{k}), \quad (2.38)$$

where  $\partial_{\parallel} = \mathbf{n} \cdot \nabla$  and  $\mu = \hat{\mathbf{k}} \cdot \mathbf{n}$ . Finally, the first-order linear relation  $\Phi = \Psi$  extends to second order for the linearly evolved PNG part of  $\Phi^{(2)}$ , giving the second equality of (2.34).

### 3 Local primordial non-Gaussianity in the relativistic bispectrum

#### 3.1 Matter bispectrum

The primordial contribution of matter, independent of halo formation, is given by the Newtonian approximation (2.15), corrected by the GR contribution in (2.22):

$$\delta_{\text{T}}^{(2)} = \delta_{\text{T,N}}^{(2)} + \delta_{\text{T,nG}}^{(2)} + \frac{20}{3} \delta_{\text{T}} \hat{\varphi}_{\text{in}} - \frac{5}{3} \xi^i \partial_i \hat{\varphi}_{\text{in}}. \quad (3.1)$$

The kernels in Fourier space corresponding to the GR terms in (3.1) are:

$$\delta_{\text{T}} \hat{\varphi}_{\text{in}} \rightarrow -\frac{(k_1^2 + k_2^2)}{2k_1^2 k_2^2}, \quad \xi^i \partial_i \hat{\varphi}_{\text{in}} \rightarrow -\frac{\mathbf{k}_1 \cdot \mathbf{k}_2}{k_1^2 k_2^2}. \quad (3.2)$$

Then the tree-level matter bispectrum  $\langle \delta_{\text{T}} \delta_{\text{T}} \delta_{\text{T}}^{(2)} \rangle$  at equal times is given by

$$B_m(\mathbf{k}_1, \mathbf{k}_2, \mathbf{k}_3) = \left\{ F_2(\mathbf{k}_1, \mathbf{k}_2) + 2f_{\text{NL}} \frac{\mathcal{M}(k_3)}{\mathcal{M}(k_1)\mathcal{M}(k_2)} - (3\Omega_m + 2f)\mathcal{H}^2 \frac{[2(k_1^2 + k_2^2) - \mathbf{k}_1 \cdot \mathbf{k}_2]}{2k_1^2 k_2^2} \right\} P(k_1)P(k_2) + 2 \text{ cp}, \quad (3.3)$$

where we omit the time dependence for brevity, and ‘cp’ denotes cyclic permutation. Here  $P \equiv P_{\text{T}}$  is the linear matter power spectrum and

$$\frac{\mathcal{M}(k_3)}{\mathcal{M}(k_1)\mathcal{M}(k_2)} = \frac{3}{10} (3\Omega_m + 2f)\mathcal{H}^2 \frac{T(k_3)}{T(k_1)T(k_2)} \frac{k_3^2}{k_1^2 k_2^2}. \quad (3.4)$$

The standard Newtonian result (see e.g. [53]) is modified in GR by the magenta terms in (3.3). For Gaussian initial conditions, the GR correction is suppressed by  $\mathcal{H}^2/k^2$  relative to the Newtonian approximation, but *in the non-Gaussian case, the GR correction is of the same order of magnitude as the local PNG term.*

#### 3.2 Observed number density

The observed number density contrast is  $\Delta_g + \Delta_g^{(2)}/2$ , which modifies the source quantity  $\delta_g + \delta_g^{(2)}/2$  by RSD and other redshift space effects. It can be split into Newtonian, relativistic and non-Gaussian parts as follows.

- The **first order** parts are:

$$\Delta_{g\text{N}} = b_{10}\delta_{\text{T,N}} - \frac{1}{\mathcal{H}}\partial_{\parallel}^2 V, \quad (3.5)$$

$$\Delta_{g\text{nG}} = b_{01}\varphi_{\text{p}}, \quad (3.6)$$

$$\begin{aligned} \Delta_{g\text{GR}} = & \left[ b_e - 2\mathcal{Q} + \frac{2(\mathcal{Q} - 1)}{\chi\mathcal{H}} - \frac{\mathcal{H}'}{\mathcal{H}^2} \right] (\partial_{\parallel} V - \Psi) \\ & + (2\mathcal{Q} - 1)\Psi + \frac{1}{\mathcal{H}}\Psi' + (3 - b_e)\mathcal{H}V. \end{aligned} \quad (3.7)$$

Recall that  $\delta_{\text{T}}$ ,  $V$  and  $\Psi$  have no GR and no PNG corrections, by (2.6) and (2.9).

- The **second-order Newtonian** part of the observed number density contrast is formed from the density contrast and RSD terms and their couplings:

$$\Delta_{gN}^{(2)} = \delta_{gT,N}^{(2)} - \frac{1}{\mathcal{H}} \partial_{\parallel}^2 V_N^{(2)} - 2 \frac{b_{10}}{\mathcal{H}} \left[ \delta_T \partial_{\parallel}^2 V + \partial_{\parallel} V \partial_{\parallel} \delta_T \right] + \frac{2}{\mathcal{H}^2} \left[ (\partial_{\parallel}^2 V)^2 + \partial_{\parallel} V \partial_{\parallel}^3 V \right]. \quad (3.8)$$

- The **second-order relativistic** part is [46, 63]:

$$\begin{aligned} \Delta_{gGR}^{(2)} = & \delta_{gT,GR}^{(2)} - \frac{1}{\mathcal{H}} \partial_{\parallel}^2 V_{GR}^{(2)} + \left[ b_e - 2\mathcal{Q} + \frac{2(\mathcal{Q}-1)}{\chi\mathcal{H}} - \frac{\mathcal{H}'}{\mathcal{H}^2} \right] \left[ \partial_{\parallel} V_{N+GR}^{(2)} - \Phi_{N+GR}^{(2)} \right] \\ & + 2(\mathcal{Q}-1)\Psi_{N+GR}^{(2)} + \Phi_{N+GR}^{(2)} + \frac{1}{\mathcal{H}} \Psi_{N+GR}^{(2)'} + (3-b_e)\mathcal{H}V_{N+GR}^{(2)} \\ & + \text{very many terms quadratic in first-order quantities,} \end{aligned} \quad (3.9)$$

where

$$V_{N+GR}^{(2)} \equiv V_N^{(2)} + V_{GR}^{(2)}, \quad (3.10)$$

and similarly for the metric potentials.

The Newtonian parts of the metric potentials  $\Psi^{(2)}, \Phi^{(2)}$  appear in the GR part of  $\Delta_g^{(2)}$  because there is *no Newtonian projection effect involving these potentials*. For the velocity potential, the Newtonian part  $V_N^{(2)}$  is present only in the RSD term in (3.8); the remaining velocity terms occur *only in the GR part* of  $\Delta_g^{(2)}$  and therefore  $V_N^{(2)}$  is included in the GR terms.

The quadratic terms in (3.9) are given in full by [46]. For convenience, Appendix A presents all of the terms in (3.9), correcting some errors in [46].

- The **second-order local PNG** part is

$$\begin{aligned} \Delta_{gnG}^{(2)} = & \delta_{gT,nG}^{(2)} - \frac{1}{\mathcal{H}} \partial_{\parallel}^2 V_{nG}^{(2)} \\ & + \left[ b_e - 2\mathcal{Q} + \frac{2(\mathcal{Q}-1)}{\chi\mathcal{H}} - \frac{\mathcal{H}'}{\mathcal{H}^2} \right] \left[ \partial_{\parallel} V_{nG}^{(2)} - \Psi_{nG}^{(2)} \right] + (2\mathcal{Q}-1)\Psi_{nG}^{(2)} + \frac{1}{\mathcal{H}} \Psi_{nG}^{(2)'} + (3-b_e)\mathcal{H}V_{nG}^{(2)} \\ & - 2 \frac{b_{01}}{\mathcal{H}} \left( \varphi_p \partial_{\parallel}^2 V + \partial_{\parallel} V \partial_{\parallel} \varphi_p \right) \\ & + b_{01} \left( c_1 \Psi \varphi_p + c_2 V \varphi_p + c_3 \varphi_p \partial_{\parallel} V + c_4 \Psi \partial_{\parallel} \varphi_p \right). \end{aligned} \quad (3.11)$$

In this expression, lines 1 and 2 contain the linearly evolved second-order terms whose nonlinearity is purely primordial. Lines 3 and 4 contain the quadratic coupling terms.

Line 1 is the Newtonian density + RSD part, given by (2.17) and (2.38).

Line 2 arises from *GR projection terms that are absent in the Newtonian approximation*: these terms are given by (2.34)–(2.38).

Line 3 arises from the first quadratic RSD term in line 2 of (3.8), given by the coupling of  $\delta_{T,nG}$  to velocity gradients.

Line 4 arises from the *coupling of  $\delta_{T,nG}$  to first-order GR projection terms*. The coefficients  $c_I(a)$  are explicitly given below and in Appendix B.

Apart from the  $b_{02}$  term in  $\delta_{gT,nG}^{(2)}$ , the Newtonian terms in (3.11) scale as  $(\mathcal{H}^2/k^2) (\delta_T)^2$  and dominate the GR correction terms, which scale as  $i(\mathcal{H}^3/k^3) (\delta_T)^2$  or  $(\mathcal{H}^4/k^4) (\delta_T)^2$ .

In summary the local PNG part at second order has the following origins:

- \* the primordial matter density contrast;
- \* the scale-dependent bias;
- \* the linearly evolved second-order projection effects in velocity and metric potentials
  - from RSD and from GR corrections;
- \* the coupling of first-order scale-dependent bias with first-order projection effects
  - from RSD and from GR corrections.

### 3.3 Galaxy bispectrum

At leading order the observed galaxy bispectrum is defined by [45]

$$2\langle\Delta_g(\mathbf{k}_1)\Delta_g(\mathbf{k}_2)\Delta_g^{(2)}(\mathbf{k}_3)\rangle + 2 \text{ cp} = (2\pi)^3 B_g(\mathbf{k}_1, \mathbf{k}_2, \mathbf{k}_3) \delta^{\text{Dirac}}(\mathbf{k}_1 + \mathbf{k}_2 + \mathbf{k}_3), \quad (3.12)$$

where here, and below, we omit the time dependence for brevity and we assume equal-time correlations. The bispectrum can be written in terms of Fourier kernels as

$$B_g(\mathbf{k}_1, \mathbf{k}_2, \mathbf{k}_3) = \mathcal{K}(\mathbf{k}_1) \mathcal{K}(\mathbf{k}_2) \mathcal{K}^{(2)}(\mathbf{k}_1, \mathbf{k}_2, \mathbf{k}_3) P(k_1) P(k_2) + 2 \text{ cp}, \quad (3.13)$$

where

$$\Delta_g(\mathbf{k}) = \mathcal{K}(\mathbf{k}) \delta_{\text{T}}(\mathbf{k}), \quad (3.14)$$

$$\Delta_g^{(2)}(\mathbf{k}_3) = \int \frac{d\mathbf{k}_1}{(2\pi)^3} d\mathbf{k}_2 \delta^{\text{Dirac}}(\mathbf{k}_1 + \mathbf{k}_2 - \mathbf{k}_3) \mathcal{K}^{(2)}(\mathbf{k}_1, \mathbf{k}_2, \mathbf{k}_3) \delta_{\text{T}}(\mathbf{k}_1) \delta_{\text{T}}(\mathbf{k}_2). \quad (3.15)$$

In [63], the Newtonian and GR kernels are presented, including all local relativistic effects, from projection, evolution and bias, but in the case of Gaussian initial conditions. Here we have updated these results and extended them to include the effects of local PNG. From Section 3.2, we find the following kernels.

- At **first order**, using (3.5)–(3.7) and (3.14):

$$\mathcal{K}_{\text{N}}(\mathbf{k}_a) = b_{10} + f\mu_a^2, \quad (3.16)$$

$$\mathcal{K}_{\text{GR}}(\mathbf{k}_a) = i\mu_a \frac{\gamma_1}{k_a} + \frac{\gamma_2}{k_a^2}, \quad (3.17)$$

$$\mathcal{K}_{\text{nG}}(\mathbf{k}_a) = \frac{b_{01}}{\mathcal{M}(k_a)}, \quad (3.18)$$

where  $\mu_a = \hat{\mathbf{k}}_a \cdot \mathbf{n}$  and

$$\frac{\gamma_1}{\mathcal{H}} = f \left[ b_e - 2\mathcal{Q} - \frac{2(1 - \mathcal{Q})}{\chi\mathcal{H}} - \frac{\mathcal{H}'}{\mathcal{H}^2} \right], \quad (3.19)$$

$$\frac{\gamma_2}{\mathcal{H}^2} = f(3 - b_e) + \frac{3}{2}\Omega_m \left[ 2 + b_e - f - 4\mathcal{Q} - \frac{2(1 - \mathcal{Q})}{\chi\mathcal{H}} - \frac{\mathcal{H}'}{\mathcal{H}^2} \right]. \quad (3.20)$$

- The **second-order Newtonian part** follows from (3.8) and (3.15) (see e.g. [36]):

$$\begin{aligned}\mathcal{K}_N^{(2)}(\mathbf{k}_1, \mathbf{k}_2, \mathbf{k}_3) = & b_{10}F_2(\mathbf{k}_1, \mathbf{k}_2) + b_{20} + f\mu_3^2G_2(\mathbf{k}_1, \mathbf{k}_2) + b_sS_2(\mathbf{k}_1, \mathbf{k}_2) \\ & + b_{10}f(\mu_1k_1 + \mu_2k_2)\left(\frac{\mu_1}{k_1} + \frac{\mu_2}{k_2}\right) + f^2\frac{\mu_1\mu_2}{k_1k_2}(\mu_1k_1 + \mu_2k_2)^2,\end{aligned}\quad (3.21)$$

where

$$G_2(\mathbf{k}_1, \mathbf{k}_2) = \frac{F'}{DD'} + \left(\frac{k_1}{k_2} + \frac{k_2}{k_1}\right)\hat{\mathbf{k}}_1 \cdot \hat{\mathbf{k}}_2 + \left(2 - \frac{F'}{DD'}\right)(\hat{\mathbf{k}}_1 \cdot \hat{\mathbf{k}}_2)^2, \quad (3.22)$$

$$S_2(\mathbf{k}_1, \mathbf{k}_2) = (\hat{\mathbf{k}}_1 \cdot \hat{\mathbf{k}}_2)^2 - \frac{1}{3}. \quad (3.23)$$

Since we use the approximation  $F/D^2 = 3/7$  in  $F_2$ , we have  $F'/(DD') = 6/7$  in  $G_2$ .

- The **second-order relativistic part** follows from (3.9) and (3.15) (see [63], with some errors that are corrected here):

$$\begin{aligned}\mathcal{K}_{\text{GR}}^{(2)}(\mathbf{k}_1, \mathbf{k}_2, \mathbf{k}_3) = & \frac{1}{k_1^2k_2^2} \left\{ \beta_1 + E_2(\mathbf{k}_1, \mathbf{k}_2, \mathbf{k}_3) \beta_2 \right. \\ & + i \left[ (\mu_1k_1 + \mu_2k_2) \beta_3 + \mu_3k_3 (\beta_4 + E_2(\mathbf{k}_1, \mathbf{k}_2, \mathbf{k}_3) \beta_5) \right] \\ & + \frac{k_1^2k_2^2}{k_3^2} \left[ F_2(\mathbf{k}_1, \mathbf{k}_2) \beta_6 + G_2(\mathbf{k}_1, \mathbf{k}_2) \beta_7 \right] + (\mu_1k_1\mu_2k_2) \beta_8 \\ & + \mu_3^2k_3^2 \left[ \beta_9 + E_2(\mathbf{k}_1, \mathbf{k}_2, \mathbf{k}_3) \beta_{10} \right] + (\mathbf{k}_1 \cdot \mathbf{k}_2) \beta_{11} \\ & + (k_1^2 + k_2^2) \beta_{12} + (\mu_1^2k_1^2 + \mu_2^2k_2^2) \beta_{13} \\ & + i \left[ (\mu_1k_1^3 + \mu_2k_2^3) \beta_{14} + (\mu_1k_1 + \mu_2k_2) (\mathbf{k}_1 \cdot \mathbf{k}_2) \beta_{15} \right. \\ & + k_1k_2 (\mu_1k_2 + \mu_2k_1) \beta_{16} + (\mu_1^3k_1^3 + \mu_2^3k_2^3) \beta_{17} \\ & \left. + \mu_1\mu_2k_1k_2 (\mu_1k_1 + \mu_2k_2) \beta_{18} + \mu_3\frac{k_1^2k_2^2}{k_3} G_2(\mathbf{k}_1, \mathbf{k}_2) \beta_{19} \right] \left. \right\},\end{aligned}\quad (3.24)$$

where

$$E_2(\mathbf{k}_1, \mathbf{k}_2, \mathbf{k}_3) = \frac{k_1^2k_2^2}{k_3^4} \left[ 3 + 2\left(\frac{k_1}{k_2} + \frac{k_2}{k_1}\right)\hat{\mathbf{k}}_1 \cdot \hat{\mathbf{k}}_2 + (\hat{\mathbf{k}}_1 \cdot \hat{\mathbf{k}}_2)^2 \right]. \quad (3.25)$$

The kernel (3.24) is derived from the many terms in  $\Delta_g^{(2)}(\mathbf{x})$ , as given in [37, 41] (we neglect the integrated terms). For convenience, in Tables 1 and 2, Appendix A, we summarise which terms in  $\Delta_g^{(2)}(\mathbf{x})$  contribute to which of the terms in (3.24). The time-dependent functions  $\beta_I$  are also given in Appendix A.

- The **second-order local PNG part** follows from (3.11):

$$\begin{aligned}
\mathcal{K}_{\text{nG}}^{(2)}(\mathbf{k}_1, \mathbf{k}_2, \mathbf{k}_3) = & 2 f_{\text{NL}}(b_{10} + f\mu_3^2) \frac{\mathcal{M}_3}{\mathcal{M}_1 \mathcal{M}_2} + f b_{01}(\mu_1 k_1 + \mu_2 k_2) \left( \frac{\mu_1}{k_1 \mathcal{M}_2} + \frac{\mu_2}{k_2 \mathcal{M}_1} \right) \\
& + b_n N_2(\mathbf{k}_1, \mathbf{k}_2) + \frac{b_{11}}{2} \left( \frac{1}{\mathcal{M}_1} + \frac{1}{\mathcal{M}_2} \right) + \frac{b_{02}}{\mathcal{M}_1 \mathcal{M}_2} \\
& + \frac{\mathcal{M}_3}{\mathcal{M}_1 \mathcal{M}_2} \left( \frac{\Upsilon_1}{k_3^2} + i \frac{\mu_3}{k_3} \Upsilon_2 \right) + \Upsilon_3 \left( \frac{1}{k_1^2 \mathcal{M}_2} + \frac{1}{k_2^2 \mathcal{M}_1} \right) \\
& + i \left[ \Upsilon_4 \left( \frac{\mu_1 k_1}{k_2^2 \mathcal{M}_1} + \frac{\mu_2 k_2}{k_1^2 \mathcal{M}_2} \right) + \Upsilon_5 \left( \frac{\mu_1}{k_1 \mathcal{M}_2} + \frac{\mu_2}{k_2 \mathcal{M}_1} \right) \right], \tag{3.26}
\end{aligned}$$

where  $\mathcal{M}_a \equiv \mathcal{M}(k_a)$  and

$$N_2(\mathbf{k}_1, \mathbf{k}_2) = \frac{1}{2} \left( \frac{k_1}{k_2 \mathcal{M}_1} + \frac{k_2}{k_1 \mathcal{M}_2} \right) \hat{\mathbf{k}}_1 \cdot \hat{\mathbf{k}}_2. \tag{3.27}$$

In the first line of (3.26), the first term is a sum of the matter density term in line 2 of (2.17) and the linearly evolved PNG part of the second-order RSD term [line 1 of (3.11)]. The second term is the quadratic RSD term from line 3 of (3.11).

The second line gives the scale-dependent bias contribution from (2.17). The first two lines recover the Newtonian approximation (see [53]).

Lines 3 and 4 in magenta are the PNG contributions that arise from relativistic projection effects, as explained in Section 3.2. These projection terms in the non-Gaussian kernel involve new time-dependent functions  $\Upsilon_I$ , which are given in Appendix B. The terms in  $\Delta_g^{(2)}(\mathbf{x})$  corresponding to those in (3.26), lines 3 and 4, are summarised in Table 3, Appendix B.

The Newtonian terms scale as  $(\mathcal{H}^2/k^2)(\delta_{\text{T}})^2$  except for the  $b_{02}$  term which scales as  $(\mathcal{H}^4/k^4)(\delta_{\text{T}})^2$ . The relativistic  $\Upsilon_1, \Upsilon_3$  terms scale as  $(\mathcal{H}^4/k^4)(\delta_{\text{T}})^2$ , while the  $\Upsilon_2, \Upsilon_4, \Upsilon_5$  terms are  $\mathcal{O}(\mathcal{H}^3/k^3)$ .

Note that  $\Upsilon_1, \Upsilon_2$  are proportional to  $f_{\text{NL}}$ , and  $\Upsilon_3, \Upsilon_4, \Upsilon_5$  are proportional to  $b_{01}$  (which itself is proportional to  $f_{\text{NL}}$ ).

For Gaussian initial conditions,  $\mathcal{K}_{\text{nG}}^{(2)}$  vanishes:

$$f_{\text{NL}} = 0 \quad \Rightarrow \quad b_{01} = b_n = b_{11} = b_{02} = \Upsilon_I = 0 \quad \Rightarrow \quad \mathcal{K}_{\text{nG}}^{(2)}(\mathbf{k}_1, \mathbf{k}_2, \mathbf{k}_3) = 0. \tag{3.28}$$

### 3.4 Numerical examples

The GR corrections to the Newtonian bispectrum, for both Gaussian and local PNG cases, are sensitive to the following astrophysical parameters of the tracer: Gaussian bias  $b_{10}$ , PNG bias  $b_{01}$ , and magnification bias  $\mathcal{Q}$ , together with their first derivatives in time and luminosity; evolution bias  $b_e$  and its first time derivative. This can be seen from the kernels presented above, with the details given in Appendices A and B.

In order to illustrate the GR corrections, we need to use physically self-consistent values for these parameters, as well as for the second-order Newtonian clustering bias parameters  $b_{20}$  and  $b_s$ . For a Stage IV H $\alpha$  spectroscopic survey, similar to Euclid, we use [66] for the clustering biases, evolution bias and magnification bias. We neglect the luminosity derivatives



of first-order clustering bias and magnification bias. For the PNG biases  $b_{11}, b_n, b_{02}$  we use (2.19)–(2.21).

We start by showing the contribution of GR corrections to the monopole of the reduced bispectrum,

$$Q_g^{00}(k_1, k_2, k_3) = \frac{B_g^{00}(k_1, k_2, k_3)}{P(k_1)P(k_2) + P(k_3)P(k_1) + P(k_2)P(k_3)}, \quad (3.29)$$

where [67]

$$B_g^{\ell m}(k_1, k_2, k_3) = \int_0^{2\pi} d\phi \int_{-1}^1 d\mu_1 B_g(k_1, k_2, k_3, \mu_1, \phi) Y_{\ell m}^*(\mu_1, \phi). \quad (3.30)$$

Here  $\phi, \mu_1$  determine the orientation of the triangle relative to the line of sight. Figure 2 shows the monopole for squeezed configurations. We use fixed equal sides  $k_1 = k_2 = 0.1 h/\text{Mpc}$  and varying long mode  $k_3 < k_1 = k_2$ . The isosceles triangle is increasingly squeezed as  $k_3$  decreases. The left panel shows the Newtonian approximation (dash-dot lines) and the right panel shows the monopole without the GR bias correction (2.27).

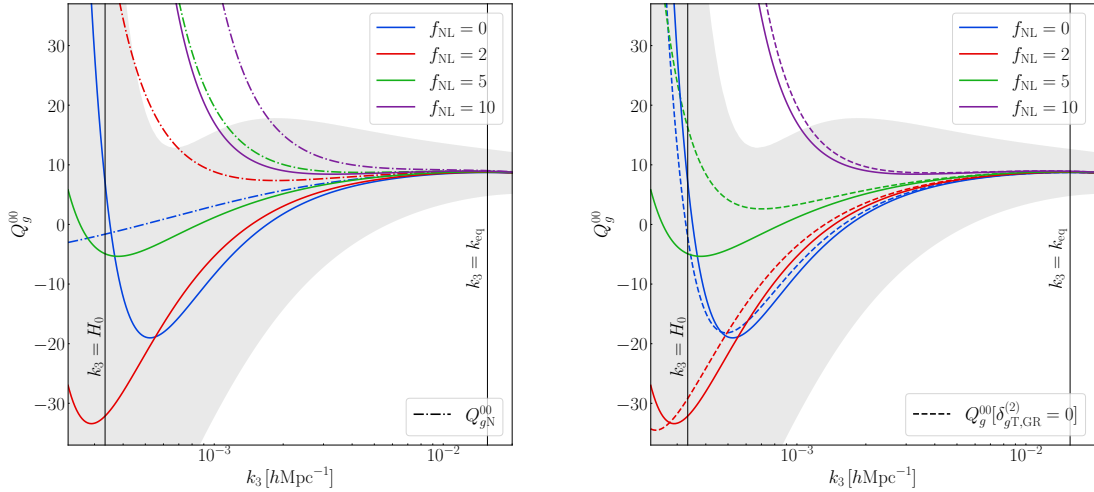


**Figure 2.** Monopole of the reduced bispectrum for a Stage IV  $\text{H}\alpha$  survey at  $z = 1$ , for various  $f_{\text{NL}}$ , with  $k_1 = k_2 = 0.1 h/\text{Mpc}$ . Shading indicates the  $1\sigma$  uncertainty (neglecting shot noise) for the  $f_{\text{NL}} = 0$  case (solid blue curve). *Left:* Comparing the full relativistic monopole to the Newtonian approximation (dash-dot curves). *Right:* Comparing the full relativistic monopole to the monopole without the GR correction to second-order galaxy bias, (2.22) (dashed curves).

The shading in Figure 2 is defined by the cosmic variance limited error  $\sigma_B$  on the  $f_{\text{NL}} = 0$  monopole, given by [77]:

$$(\sigma_B)^2 = \frac{\mathcal{V}^{\text{com}}}{\pi k_1 k_2 k_3 \Delta k} \int d\mu_1 d\phi P_g(k_1, \mu_1) P_g(k_2, \mu_2) P_g(k_3, \mu_3), \quad (3.31)$$

where the galaxy power spectrum, from (3.16)–(3.18), is

$$P_g(k_a, \mu_a) = \left| b_{10} + f\mu_a^2 + \frac{\gamma_2}{k_a^2} + i\mu_a \frac{\gamma_1}{k_a} \right|^2 P(k_a). \quad (3.32)$$

In (3.31),  $\mathcal{V}^{\text{com}}$  is the comoving volume of the redshift bin,  $\Delta k$  is chosen as the fundamental mode,  $2\pi(\mathcal{V}^{\text{com}})^{-1/3}$ ,  $k_1 = k_2 = 0.1 h/\text{Mpc}$ , and [65]  $\mu_2 = \mu_1 \cos \theta_{12} + \sqrt{1 - \mu_1^2} \sin \theta_{12} \cos \phi$ ,  $\mu_3 = -(k_1 \mu_1 + k_2 \mu_2)/k_3$ . Here  $\theta_{12}$  is the tail-to-tail angle between  $\mathbf{k}_1$  and  $\mathbf{k}_2$ , so that the squeezed limit is  $\theta_{12} = \pi$ .

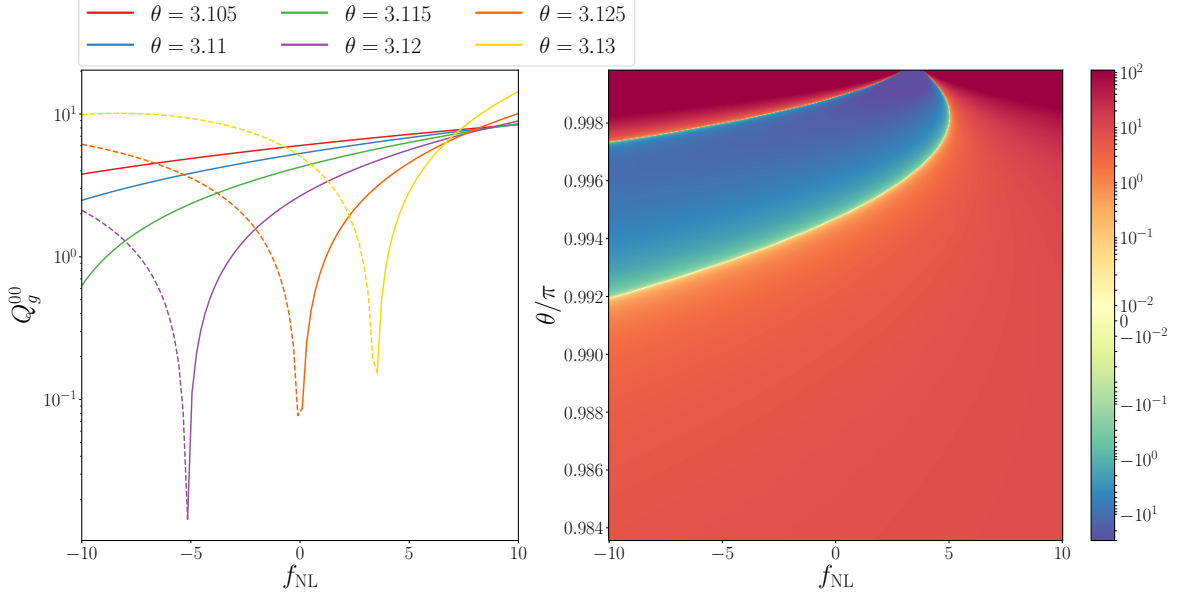


**Figure 3.** Monopole of reduced bispectrum for isosceles triangles, as in Figure 2. *Left:* As a function of  $f_{\text{NL}}$ , for various values of  $\theta \equiv \theta_{12}$ , where  $\theta = \pi$  is the squeezed limit. Dashed curves indicate negative values. *Right:* 2D colour map as a function of  $f_{\text{NL}}$  and  $\theta/\pi$ .

The effect of  $f_{\text{NL}}$  is strongest in the monopole and competes with the GR contribution on ultra-large scales, since they both affect the Newtonian Gaussian bispectrum at  $\mathcal{O}(\mathcal{H}^2/k^2)$ . We see this in Figure 2 left panel, which shows the monopole of the reduced bispectrum for an increasingly squeezed isosceles triangle. In the Gaussian case (blue) we see that the Newtonian reduced monopole (dot-dash blue) becomes negative when the long mode is close to the Hubble scale, due to the effects of second-order galaxy bias. The Gaussian GR correction to the Newtonian approximation is negative for super-equality long modes until close to the Hubble scale (this was pointed out in [64]). GR effects drive the reduced monopole (solid blue) below zero for  $H_0 \lesssim k_3 \lesssim 0.002 h/\text{Mpc}$  (the locations of the zero-crossings are dependent on the Gaussian bias parameters, evolution bias and magnification bias).

As  $f_{\text{NL}}$  is increased above zero, the amplitude of the Newtonian reduced monopole (dot-dash curves) increases monotonically. When GR effects are taken into account, the reduced monopole is pushed upwards, but remains negative on observable scales for  $f_{\text{NL}} \lesssim 5$ , until it becomes always positive for  $f_{\text{NL}} > 5$  – the precise turnaround value of  $f_{\text{NL}}$  depends on astrophysical parameters. This means that for  $f_{\text{NL}} \lesssim 5$ , local PNG *decreases* the amplitude of the reduced monopole on observable scales, in contrast to the Newtonian approximation. Comparing the green solid and blue dot-dash curves shows that *the Newtonian approximation is very close to the true reduced monopole with  $f_{\text{NL}} \sim 5$* . For a universe with  $f_{\text{NL}} \sim 5$ , a Newtonian analysis of the squeezed bispectrum would conclude that the primordial universe is Gaussian. Similarly, a universe with  $f_{\text{NL}} \sim 10$  would appear to have  $f_{\text{NL}} \sim 5$  in a Newtonian approximation.

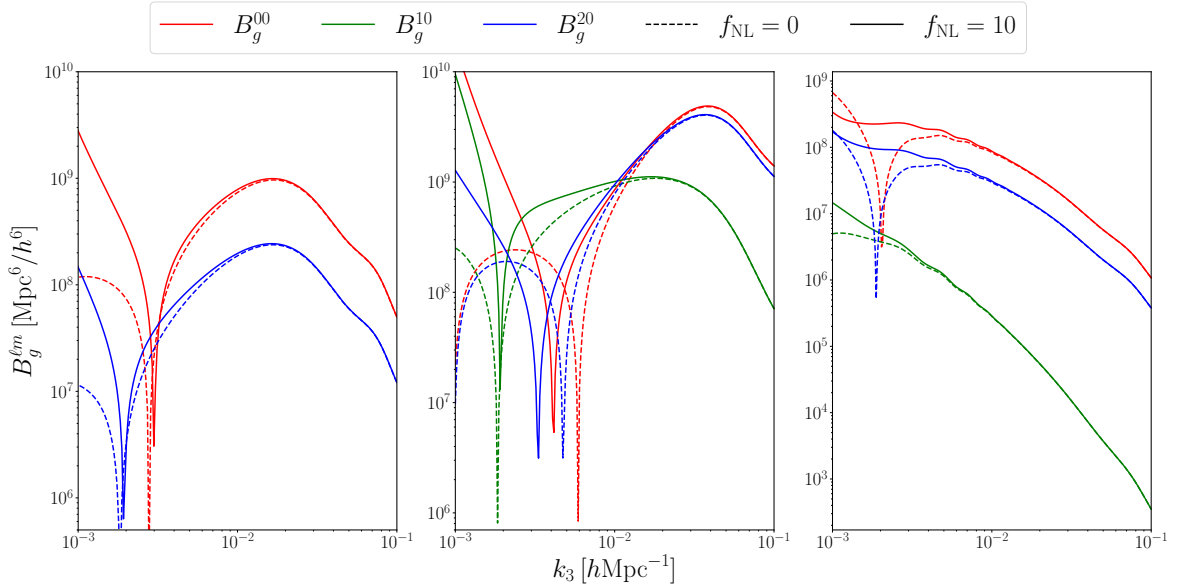


**Figure 4.** First few nonzero multipoles for fixed triangle shape as a function of  $k_3$ , with  $f_{\text{NL}} = 10$  (solid) and  $f_{\text{NL}} = 0$  (dashed). *Left:* Equilateral configuration,  $k_1 = k_2 = k_3$ . *Middle:* Flattened configuration,  $k_1 = k_2 \approx k_3/2$ , with  $\theta_{12} = 2^\circ$ . *Right:* Squeezed configuration with  $\theta_{12} = 178^\circ$  and  $k_1 = k_2 = k_3/(2 \sin \theta_{12}) \approx 14 k_3$ .

The GR contribution to the monopole is made up of:  $\mathcal{O}(\mathcal{H}^2/k^2)$  Gaussian projection terms,  $\mathcal{O}(\mathcal{H}^2/k^2)$  second-order galaxy bias correction (the same for Gaussian and PNG cases) and  $\mathcal{O}(\mathcal{H}^4/k^4)$  second-order local PNG contributions from GR projection effects. The last contribution is effectively negligible on observable scales. In the right panel of Figure 2 we show that the GR bias correction is dominated by the Gaussian GR projection terms: the effect of removing the GR correction to second-order galaxy bias is small. Note that the GR bias correction has a similar effect to a small negative value of  $f_{\text{NL}}$ .

In Figure 3 we include negative  $f_{\text{NL}}$  and explore how local PNG changes the monopole of the reduced bispectrum as we approach the squeezed limit,  $\theta_{12} \rightarrow \pi$ . For  $f_{\text{NL}} \geq 0$ , the results provide a different perspective on Figure 2 left panel. For negative  $f_{\text{NL}}$ , local PNG and GR effects act together to drive the monopole negative, so that the zero-crossing of the monopole occurs for smaller  $\theta_{12}$ , equivalently larger  $k_3$ .

Figure 4 shows the effect of  $f_{\text{NL}}$  on the first three multipoles of the relativistic galaxy bispectrum, also including equilateral and flattened triangle shapes. In general, the Newtonian RSD effect induces only even multipoles, while the GR corrections modify the even multipoles and induce new odd multipoles. We show here the  $m = 0$  dipole (absent without GR corrections) and quadrupole (mainly Newtonian), compared to the monopole.

For the equilateral shape (left panel), the dipole vanishes exactly in the Gaussian case [65, 67] and nonzero  $f_{\text{NL}}$  does not change this result. The effect of  $f_{\text{NL}}$  on the quadrupole is very similar to the case of the monopole.

For the flattened shape (middle panel), the dipole is the dominant part of the bispectrum for  $0.002 \lesssim k_3/(h\text{Mpc}^{-1}) \lesssim 0.01$ , and we see that  $f_{\text{NL}} > 0$  increases this effect further. The dipole  $B_g^{1m}$  is purely relativistic: it vanishes in the Newtonian approximation [13, 65, 66].

Finally, in the squeezed case (right panel), the effect on the monopole of  $f_{\text{NL}} = 10$  is consistent with Figure 2. The quadrupole has a similar behaviour, and dominates the

dipole. It is interesting that the three multipoles are approximately equal at scales near  $k = 0.002 h/\text{Mpc}$ . Once again, this value is sensitive to astrophysical parameters.

## 4 Conclusions

Upcoming galaxy surveys and 21cm intensity mapping surveys will deliver high-precision cosmological measurements and constraints, based on a combination of the power spectrum and bispectrum. This advance demands a commensurate advance in theoretical precision. Here we contribute to the development of theoretical precision by deriving for the first time the local relativistic corrections to the tree-level redshift-space bispectrum in the presence of local primordial non-Gaussianity (PNG).

At first order in perturbations, there are no relativistic corrections to the comoving matter and galaxy density contrasts – and therefore no correction to the galaxy clustering bias relation. There are also no relativistic corrections to the velocity and metric potentials. Consequently, there is no relativistic contribution to local PNG. The only relativistic correction is to the Newtonian projection effect, i.e. standard redshift-space distortions (RSD).

At second-order, relativistic corrections go beyond projection effects to alter the galaxy bias relation and local PNG in the galaxy bispectrum. In summary, there are:

- relativistic projection corrections to the Newtonian RSD at first and second order;
- relativistic corrections to the Newtonian bias model in the comoving frame at second order;
- second-order relativistic projection corrections to the local PNG carried by Newtonian RSD – from a coupling of first-order scale-dependent bias to first-order relativistic projection effects, and from the linearly evolved local PNG in second-order velocity and metric potentials.

Our previous work [13, 45, 46, 63–67] presented local (non-integrated) relativistic effects in the case of primordial Gaussianity and without the relativistic correction to galaxy bias. We have made corrections to these earlier results. In addition, we have presented for the first time the galaxy bispectrum with relativistic corrections to galaxy clustering bias and new local PNG contributions that are encoded in relativistic projection effects. Our main results are given in Fourier space in (3.21)–(3.26), with further details in Appendices A and B.

In Figures 2 and 3 we show examples of the squeezed monopole of the reduced relativistic bispectrum for a Stage IV  $\text{H}\alpha$  survey similar to Euclid, using physical models for the astrophysical parameters (clustering biases, evolution bias, magnification bias). These figures reveal various interesting relativistic features. In particular, they show the bias in the estimate of  $f_{\text{NL}}$  from using a Newtonian analysis. This bias is given by

$$f_{\text{NL}}^{\text{Newt}} = f_{\text{NL}} + \Delta f_{\text{NL}}. \quad (4.1)$$

For the Stage IV survey at  $z = 1$ , the bias can be roughly estimated by eye as  $\Delta f_{\text{NL}} \sim 5$ , for the long mode above the equality scale. Although the precise level of bias is sensitive to astrophysical parameters and redshift, the point is that next-generation precision demands that relativistic corrections are included in the bispectrum.

**Acknowledgements**

We thank Kazuya Koyama for very useful discussions. RM and SJ are supported by the South African Radio Astronomy Observatory (SARAO) and the National Research Foundation (Grant No. 75415). RM and OU are supported by the UK Science & Technology Facilities Council (STFC) Consolidated Grant ST/S000550/1. CC is supported by STFC Consolidated Grant ST/P000592/1.

## A $\beta_I$ functions in (3.24)

$$\begin{aligned}
\frac{\beta_1}{\mathcal{H}^4} = & \frac{9}{4}\Omega_m^2 \left[ 6 - 2f \left( 2b_e - 4\mathcal{Q} - \frac{4(1-\mathcal{Q})}{\chi\mathcal{H}} - \frac{2\mathcal{H}'}{\mathcal{H}^2} \right) - \frac{2f'}{\mathcal{H}} + b_e^2 + 5b_e - 8b_e\mathcal{Q} + 4\mathcal{Q} + 16\mathcal{Q}^2 \right. \\
& - 16\frac{\partial\mathcal{Q}}{\partial\ln L} - 8\frac{\mathcal{Q}'}{\mathcal{H}} + \frac{b_e'}{\mathcal{H}} + \frac{2}{\chi^2\mathcal{H}^2} \left( 1 - \mathcal{Q} + 2\mathcal{Q}^2 - 2\frac{\partial\mathcal{Q}}{\partial\ln L} \right) \\
& - \frac{2}{\chi\mathcal{H}} \left( 3 + 2b_e - 2b_e\mathcal{Q} - 3\mathcal{Q} + 8\mathcal{Q}^2 - \frac{3\mathcal{H}'}{\mathcal{H}^2}(1-\mathcal{Q}) - 8\frac{\partial\mathcal{Q}}{\partial\ln L} - 2\frac{\mathcal{Q}'}{\mathcal{H}} \right) \\
& \left. + \frac{\mathcal{H}'}{\mathcal{H}^2} \left( -7 - 2b_e + 8\mathcal{Q} + \frac{3\mathcal{H}'}{\mathcal{H}^2} \right) - \frac{\mathcal{H}''}{\mathcal{H}^3} \right] \\
& + \frac{3}{2}\Omega_m f \left[ 5 - 2f(4 - b_e) + \frac{2f'}{\mathcal{H}} + 2b_e \left( 5 + \frac{2(1-\mathcal{Q})}{\chi\mathcal{H}} \right) - \frac{2b_e'}{\mathcal{H}} - 2b_e^2 + 8b_e\mathcal{Q} - 28\mathcal{Q} \right. \\
& \left. - \frac{14(1-\mathcal{Q})}{\chi\mathcal{H}} - \frac{3\mathcal{H}'}{\mathcal{H}^2} + 4 \left( 2 - \frac{1}{\chi\mathcal{H}} \right) \frac{\mathcal{Q}'}{\mathcal{H}} \right] \\
& + \frac{3}{2}\Omega_m f^2 \left[ -2 + 2f - b_e + 4\mathcal{Q} + \frac{2(1-\mathcal{Q})}{\chi\mathcal{H}} + \frac{3\mathcal{H}'}{\mathcal{H}^2} \right] \\
& + f^2 \left[ 12 - 7b_e + b_e^2 + \frac{b_e'}{\mathcal{H}} + (b_e - 3)\frac{\mathcal{H}'}{\mathcal{H}^2} \right] - \frac{3}{2}\Omega_m \frac{f'}{\mathcal{H}}
\end{aligned} \tag{A.1}$$

$$\begin{aligned}
\frac{\beta_2}{\mathcal{H}^4} = & \frac{9}{2}\Omega_m^2 \left[ -1 + b_e - 2\mathcal{Q} - \frac{2(1-\mathcal{Q})}{\chi\mathcal{H}} - \frac{\mathcal{H}'}{\mathcal{H}^2} \right] + 3\Omega_m f \left[ -1 + 2f - b_e + 4\mathcal{Q} + \frac{2(1-\mathcal{Q})}{\chi\mathcal{H}} + \frac{3\mathcal{H}'}{\mathcal{H}^2} \right] \\
& + 3\Omega_m f^2 \left[ -1 + b_e - 2\mathcal{Q} - \frac{2(1-\mathcal{Q})}{\chi\mathcal{H}} - \frac{\mathcal{H}'}{\mathcal{H}^2} \right] + 3\Omega_m \frac{f'}{\mathcal{H}}
\end{aligned} \tag{A.2}$$

$$\begin{aligned}
\frac{\beta_3}{\mathcal{H}^3} = & \frac{9}{4}\Omega_m^2 (f - 2 + 2\mathcal{Q}) + \frac{3}{2}\Omega_m f \left[ -2 - f \left( -3 + f + 2b_e - 3\mathcal{Q} - \frac{4(1-\mathcal{Q})}{\chi\mathcal{H}} - \frac{2\mathcal{H}'}{\mathcal{H}^2} \right) - \frac{f'}{\mathcal{H}} \right. \\
& + 3b_e + b_e^2 - 6b_e\mathcal{Q} + 4\mathcal{Q} + 8\mathcal{Q}^2 - 8\frac{\partial\mathcal{Q}}{\partial\ln L} - 6\frac{\mathcal{Q}'}{\mathcal{H}} + \frac{b_e'}{\mathcal{H}} \\
& + \frac{2}{\chi^2\mathcal{H}^2} \left( 1 - \mathcal{Q} + 2\mathcal{Q}^2 - 2\frac{\partial\mathcal{Q}}{\partial\ln L} \right) + \frac{2}{\chi\mathcal{H}} \left( -1 - 2b_e + 2b_e\mathcal{Q} + \mathcal{Q} - 6\mathcal{Q}^2 \right. \\
& \left. + \frac{3\mathcal{H}'}{\mathcal{H}^2}(1-\mathcal{Q}) + 6\frac{\partial\mathcal{Q}}{\partial\ln L} + 2\frac{\mathcal{Q}'}{\mathcal{H}} \right) - \frac{\mathcal{H}'}{\mathcal{H}^2} \left( 3 + 2b_e - 6\mathcal{Q} - \frac{3\mathcal{H}'}{\mathcal{H}^2} \right) - \frac{\mathcal{H}''}{\mathcal{H}^3} \left. \right] \\
& + f^2 \left[ -3 + 2b_e \left( 2 + \frac{(1-\mathcal{Q})}{\chi\mathcal{H}} \right) - b_e^2 + 2b_e\mathcal{Q} - 6\mathcal{Q} - \frac{b_e'}{\mathcal{H}} - \frac{6(1-\mathcal{Q})}{\chi\mathcal{H}} + 2 \left( 1 - \frac{1}{\chi\mathcal{H}} \right) \frac{\mathcal{Q}'}{\mathcal{H}} \right]
\end{aligned} \tag{A.3}$$

$$\frac{\beta_4}{\mathcal{H}^3} = \frac{9}{2}\Omega_m f \left[ -b_e + 2\mathcal{Q} + \frac{2(1-\mathcal{Q})}{\chi\mathcal{H}} + \frac{\mathcal{H}'}{\mathcal{H}^2} \right] \tag{A.4}$$

$$\frac{\beta_5}{\mathcal{H}^3} = 3\Omega_m f \left[ b_e - 2\mathcal{Q} - \frac{2(1-\mathcal{Q})}{\chi\mathcal{H}} - \frac{\mathcal{H}'}{\mathcal{H}^2} \right] \tag{A.5}$$

$$\frac{\beta_6}{\mathcal{H}^2} = \frac{3}{2}\Omega_m \left[ 2 - 2f + b_e - 4\mathcal{Q} - \frac{2(1-\mathcal{Q})}{\chi\mathcal{H}} - \frac{\mathcal{H}'}{\mathcal{H}^2} \right] \tag{A.6}$$

$$\frac{\beta_7}{\mathcal{H}^2} = f(3 - b_e) \quad (\text{A.7})$$

$$\begin{aligned} \frac{\beta_8}{\mathcal{H}^2} = & 3\Omega_m f(2 - f - 2\mathcal{Q}) + f^2 \left[ 4 + b_e - b_e^2 + 4b_e\mathcal{Q} - 6\mathcal{Q} - 4\mathcal{Q}^2 + 4\frac{\partial\mathcal{Q}}{\partial\ln L} + 4\frac{\mathcal{Q}'}{\mathcal{H}} - \frac{b_e'}{\mathcal{H}} \right. \\ & - \frac{2}{\chi^2\mathcal{H}^2} \left( 1 - \mathcal{Q} + 2\mathcal{Q}^2 - 2\frac{\partial\mathcal{Q}}{\partial\ln L} \right) - \frac{2}{\chi\mathcal{H}} \left( 3 - 2b_e + 2b_e\mathcal{Q} - \mathcal{Q} - 4\mathcal{Q}^2 + \frac{3\mathcal{H}'}{\mathcal{H}^2} (1 - \mathcal{Q}) \right. \\ & \left. \left. + 4\frac{\partial\mathcal{Q}}{\partial\ln L} + 2\frac{\mathcal{Q}'}{\mathcal{H}} \right) - \frac{\mathcal{H}'}{\mathcal{H}^2} \left( 3 - 2b_e + 4\mathcal{Q} + \frac{3\mathcal{H}'}{\mathcal{H}^2} \right) + \frac{\mathcal{H}''}{\mathcal{H}^3} \right] \end{aligned} \quad (\text{A.8})$$

$$\frac{\beta_9}{\mathcal{H}^2} = -\frac{9}{2}\Omega_m f \quad (\text{A.9})$$

$$\frac{\beta_{10}}{\mathcal{H}^2} = 3\Omega_m f \quad (\text{A.10})$$

$$\frac{\beta_{11}}{\mathcal{H}^2} = \frac{3}{2}\Omega_m \left( 1 + \frac{2f}{3\Omega_m} \right) + 3\Omega_m f - f^2 \left[ -1 + b_e - 2\mathcal{Q} - \frac{2(1-\mathcal{Q})}{\chi\mathcal{H}} - \frac{\mathcal{H}'}{\mathcal{H}^2} \right] \quad (\text{A.11})$$

$$\begin{aligned} \frac{\beta_{12}}{\mathcal{H}^2} = & -3\Omega_m \left( 1 + \frac{2f}{3\Omega_m} \right) - f \left[ b_{10}(f - 3 + b_e) + \frac{b_{10}'}{\mathcal{H}} \right] \\ & + \frac{3}{2}\Omega_m \left[ b_{10} \left( 2 + b_e - 4\mathcal{Q} - \frac{2(1-\mathcal{Q})}{\chi\mathcal{H}} - \frac{\mathcal{H}'}{\mathcal{H}^2} \right) + \frac{b_{10}'}{\mathcal{H}} + 2 \left( 2 - \frac{1}{\chi\mathcal{H}} \right) \frac{\partial b_{10}}{\partial\ln L} \right] \end{aligned} \quad (\text{A.12})$$

$$\frac{\beta_{13}}{\mathcal{H}^2} = \frac{9}{4}\Omega_m^2 + \frac{3}{2}\Omega_m f \left[ 1 - 2f + 2b_e - 6\mathcal{Q} - \frac{4(1-\mathcal{Q})}{\chi\mathcal{H}} - \frac{3\mathcal{H}'}{\mathcal{H}^2} \right] + f^2(3 - b_e) \quad (\text{A.13})$$

$$\frac{\beta_{14}}{\mathcal{H}} = -\frac{3}{2}\Omega_m b_{10} \quad (\text{A.14})$$

$$\frac{\beta_{15}}{\mathcal{H}} = 2f^2 \quad (\text{A.15})$$

$$\frac{\beta_{16}}{\mathcal{H}} = f \left[ b_{10} \left( f + b_e - 2\mathcal{Q} - \frac{2(1-\mathcal{Q})}{\chi\mathcal{H}} - \frac{\mathcal{H}'}{\mathcal{H}^2} \right) + \frac{b_{10}'}{\mathcal{H}} + 2 \left( 1 - \frac{1}{\chi\mathcal{H}} \right) \frac{\partial b_{10}}{\partial\ln L} \right] \quad (\text{A.16})$$

$$\frac{\beta_{17}}{\mathcal{H}} = -\frac{3}{2}\Omega_m f \quad (\text{A.17})$$

$$\frac{\beta_{18}}{\mathcal{H}} = \frac{3}{2}\Omega_m f - f^2 \left[ 3 - 2b_e + 4\mathcal{Q} + \frac{4(1-\mathcal{Q})}{\chi\mathcal{H}} + \frac{3\mathcal{H}'}{\mathcal{H}^2} \right] \quad (\text{A.18})$$

$$\frac{\beta_{19}}{\mathcal{H}} = f \left[ b_e - 2\mathcal{Q} - \frac{2(1-\mathcal{Q})}{\chi\mathcal{H}} - \frac{\mathcal{H}'}{\mathcal{H}^2} \right] \quad (\text{A.19})$$

**Table 1.** Individual terms in the observed  $\Delta_g^{(2)}(a, \mathbf{x})$  [see (3.8), (3.9)] for  $f_{\text{NL}} = 0$  are shown in column 1. The related  $\beta_I$  functions in (3.24) are listed in column 2. The Fourier-space kernels  $\mathcal{F}$  corresponding to column 1, given by  $\int d\mathbf{k}' \mathcal{F}(\mathbf{k}', \mathbf{k} - \mathbf{k}') \delta_{\text{T}}(\mathbf{k}') \delta_{\text{T}}(\mathbf{k} - \mathbf{k}') / (2\pi)^3$ , are shown in column 3. Column 4 gives the coefficients of the terms in  $\Delta_g^{(2)}$  (column 1). The line-of-sight derivative is  $\partial_{\parallel} = \mathbf{n} \cdot \nabla$  and  $\Phi = \Psi$ . The superscript (1) on first-order quantities has been omitted and N denotes Newtonian. This table updates the one in [46].

TERM	$\beta$	FOURIER KERNEL	COEFFICIENT
$\delta_{\text{T},\text{N}}^{(2)}$	N	$F_2(\mathbf{k}_1, \mathbf{k}_2)$	$b_{10}$
$(\delta_{\text{T}})^2$	N	1	$b_{20}$
$s^2$	N	$S_2(\mathbf{k}_1, \mathbf{k}_2)$	$b_s$
$\partial_{\parallel}^2 V_{\text{N}}^{(2)}$	N	$f^2 \mathcal{H} \mu_3^2 G_2(\mathbf{k}_1, \mathbf{k}_2)$	$-1/\mathcal{H}$
$\delta_{\text{T}} \partial_{\parallel}^2 V$	N	$-f \mathcal{H} (\mu_1^2 + \mu_2^2)/2$	$-2b_{10}/\mathcal{H}$
$\partial_{\parallel} V \partial_{\parallel} \delta_{\text{T}}$	N	$-f \mathcal{H} \mu_1 \mu_2 (k_1^2 + k_2^2)/(2k_1 k_2)$	$-2b_{10}/\mathcal{H}$
$\partial_{\parallel} V \partial_{\parallel}^3 V$	N	$f^2 \mathcal{H}^2 (\mu_1 \mu_2^3 k_2^2 + \mu_2 \mu_1^3 k_1^2)/(k_1 k_2)$	$2/\mathcal{H}^2$
$[\partial_{\parallel}^2 V]^2$	N	$f^2 \mathcal{H}^2 \mu_1^2 \mu_2^2$	$2/\mathcal{H}^2$
$(\Psi)^2$	$\beta_1$	$9\Omega_m^2 \mathcal{H}^4 / (4k_1^2 k_2^2)$	$\mathcal{A}_1$
$\Psi V$	$\beta_1$	$-3\Omega_m \mathcal{H}^3 f / (2k_1^2 k_2^2)$	$\mathcal{A}_2$
$V V'$	$\beta_1$	$f \mathcal{H}^3 (3\Omega_m - 2f) / (2k_1^2 k_2^2)$	$(b_e - 3)\mathcal{H}$
$(V)^2$	$\beta_1$	$f^2 \mathcal{H}^2 / (k_1^2 k_2^2)$	$(b_e - 3)^2 \mathcal{H}^2 + b'_e \mathcal{H} + (b_e - 3)\mathcal{H}'$
$V_{\text{GR}}^{(2)}$	$\beta_1, \beta_2$	$-3\Omega_m \mathcal{H}^3 [3 - 2E_2(\mathbf{k}_1, \mathbf{k}_2, \mathbf{k}_3)] / (4k_1^2 k_2^2)$	$(3 - b_e)\mathcal{H}$
$\Phi_{\text{GR}}^{(2)}$	$\beta_1, \beta_2$	$3\Omega_m \mathcal{H}^4 [f - C_1 + C_1 E_2(\mathbf{k}_1, \mathbf{k}_2, \mathbf{k}_3)] / (2k_1^2 k_2^2)$	$1 - b_e + 2\mathcal{Q} + \mathcal{R}$
$\Psi_{\text{GR}}^{(2)}$	$\beta_1, \beta_2$	$3\Omega_m \mathcal{H}^4 [C_1 - 3f + 2f^2 + 2f E_2(\mathbf{k}_1, \mathbf{k}_2, \mathbf{k}_3)] / (2k_1^2 k_2^2)$	$2(\mathcal{Q} - 1)$
$\Psi_{\text{GR}}^{(2)'} = \Phi_{\text{GR}}^{(2)'}$	$\beta_1, \beta_2$	$3\Omega_m \mathcal{H}^5 [C_2 + C_3 E_2(\mathbf{k}_1, \mathbf{k}_2, \mathbf{k}_3)] / (2k_1^2 k_2^2)$	$1/\mathcal{H}$
$V \partial_{\parallel} V$	$\beta_3$	$i f^2 \mathcal{H}^2 (\mu_1 k_1 + \mu_2 k_2) / (2k_1^2 k_2^2)$	$\mathcal{A}_3$
$\Psi \partial_{\parallel} V$	$\beta_3$	$-i 3f \Omega_m \mathcal{H}^3 (\mu_1 k_1 + \mu_2 k_2) / (4k_1^2 k_2^2)$	$\mathcal{A}_4$
$\Psi \partial_{\parallel} \Phi$	$\beta_3$	$i 9\Omega_m^2 \mathcal{H}^4 (\mu_1 k_1 + \mu_2 k_2) / (8k_1^2 k_2^2)$	$2(f - 2 + 2\mathcal{Q})/\mathcal{H}$
$\partial_{\parallel} V_{\text{GR}}^{(2)}$	$\beta_4, \beta_5$	$-i 3\Omega_m \mathcal{H}^3 [3 - 2E_2(\mathbf{k}_1, \mathbf{k}_2, \mathbf{k}_3)] \mu_3 k_3 / (4k_1^2 k_2^2)$	$b_e - 2\mathcal{Q} - \mathcal{R}$
$\Psi_{\text{N}}^{(2)} = \Phi_{\text{N}}^{(2)}$	$\beta_6$	$-3\Omega_m \mathcal{H}^2 F_2(\mathbf{k}_1, \mathbf{k}_2) / (2k_3^2)$	$4\mathcal{Q} - 1 - b_e + \mathcal{R}$
$\Psi_{\text{N}}^{(2)'} = \Phi_{\text{N}}^{(2)'}$	$\beta_6$	$-3\Omega_m \mathcal{H}^3 (2f - 1) F_2(\mathbf{k}_1, \mathbf{k}_2) / (2k_3^2)$	$1/\mathcal{H}$
$V_{\text{N}}^{(2)}$	$\beta_7$	$f \mathcal{H} G_2(\mathbf{k}_1, \mathbf{k}_2) / k_3^2$	$(3 - b_e)\mathcal{H}$
$(\partial_{\parallel} V)^2$	$\beta_8$	$-f^2 \mathcal{H}^2 \mu_1 \mu_2 / (k_1 k_2)$	$\mathcal{A}_5$
$\partial_{\parallel} V \partial_{\parallel} \Psi$	$\beta_8$	$3f \Omega_m \mathcal{H}^3 \mu_1 \mu_2 / (2k_1 k_2)$	$2(2 - f - 2\mathcal{Q})/\mathcal{H}$
$\partial_{\parallel}^2 V_{\text{GR}}^{(2)}$	$\beta_9, \beta_{10}$	$i 3\Omega_m \mathcal{H}^3 [3 - 2E_2(\mathbf{k}_1, \mathbf{k}_2, \mathbf{k}_3)] \mu_3^2 k_3^2 / (4k_1^2 k_2^2)$	$-1/\mathcal{H}$
$\partial_i V \partial^i V$	$\beta_{11}$	$-f^2 \mathcal{H}^2 \mathbf{k}_1 \cdot \mathbf{k}_2 / (k_1^2 k_2^2)$	$b_e - 1 - 2\mathcal{Q} - \mathcal{R}$
$\partial_i V \partial^i \Psi$	$\beta_{11}$	$3f \Omega_m \mathcal{H}^3 \mathbf{k}_1 \cdot \mathbf{k}_2 / (2k_1^2 k_2^2)$	$2/\mathcal{H}$
$\Psi \delta_{\text{T}}$	$\beta_{12}$	$-3\Omega_m \mathcal{H}^2 (k_1^2 + k_2^2) / (4k_1^2 k_2^2)$	$2b_{10}(4\mathcal{Q} + \mathcal{R} - 2 - b_e) - \mathcal{S}$
$V \delta_{\text{T}}$	$\beta_{12}$	$f \mathcal{H} (k_1^2 + k_2^2) / (2k_1^2 k_2^2)$	$b'_{10} + 2b_{10}(3 - b_e - f)\mathcal{H}$



**Table 2.** Table 1 continued.

TERM	$\beta$	FOURIER KERNEL	COEFFICIENT
$\delta_{gT,GR}^{(2)}$	$\beta_{11}, \beta_{12}$	$(3\Omega_m + 2f)\mathcal{H}^2[\mathbf{k}_1 \cdot \mathbf{k}_2 - 2(k_1^2 + k_2^2)]/(2k_1 k_2)$	1
$\Psi \partial_{\parallel}^2 V$	$\beta_{13}$	$3f\Omega_m \mathcal{H}^3(\mu_1^2 k_1^2 + \mu_2^2 k_2^2)/(4k_1^2 k_2^2)$	$2[1 - 2f + 2b_e - 6\mathcal{Q} - 2\mathcal{R} - (\mathcal{H}'/\mathcal{H}^2)]/\mathcal{H}$
$\Psi \partial_{\parallel}^2 \Psi$	$\beta_{13}$	$-9\Omega_m^2 \mathcal{H}^4(\mu_1^2 k_1^2 + \mu_2^2 k_2^2)/(4k_1^2 k_2^2)$	$-2/\mathcal{H}^2$
$V \partial_{\parallel}^2 V$	$\beta_{13}$	$-f^2 \mathcal{H}^3(\mu_1^2 k_1^2 + \mu_2^2 k_2^2)/(2k_1^2 k_2^2)$	$2(b_e - 3)/\mathcal{H}$
$\Psi \partial_{\parallel} \delta_T$	$\beta_{14}$	$-i 3\Omega_m \mathcal{H}^2(\mu_1 k_1^3 + \mu_2 k_2^3)/(4k_1^2 k_2^2)$	$2b_{10}/\mathcal{H}$
$\partial_i V \partial_{\parallel} \partial^i V$	$\beta_{15}$	$-i f^2 \mathcal{H}^2 \mathbf{k}_1 \cdot \mathbf{k}_2 (\mu_1 k_1 + \mu_2 k_2)/(2k_1^2 k_2^2)$	$-4/\mathcal{H}$
$\delta_T \partial_{\parallel} V$	$\beta_{16}$	$i f \mathcal{H}(\mu_1 k_2 + \mu_2 k_1)/(2k_1 k_2)$	$2b_{10}(f + b_e - 2\mathcal{Q} - \mathcal{R}) + \mathcal{S}$
$\Phi \partial_{\parallel}^3 V$	$\beta_{17}$	$i 3f\Omega_m \mathcal{H}^3(\mu_1^3 k_1^3 + \mu_2^3 k_2^3)/(4k_1^2 k_2^2)$	$-2/\mathcal{H}^2$
$\partial_{\parallel} V \partial_{\parallel}^2 V$	$\beta_{18}$	$-i f^2 \mathcal{H}^2(\mu_1 \mu_2^2 k_2 + \mu_2 \mu_1^2 k_1)/(2k_1 k_2)$	$2[3 - 2b_e + 4\mathcal{Q} + 2\mathcal{R} + (\mathcal{H}'/\mathcal{H}^2)]/\mathcal{H}$
$\partial_{\parallel} V \partial_{\parallel}^2 \Psi$	$\beta_{18}$	$i 3f\Omega_m \mathcal{H}^3(\mu_1 \mu_2^2 k_2 + \mu_2 \mu_1^2 k_1)/(4k_1 k_2)$	$2/\mathcal{H}^2$
$\partial_{\parallel} V_N^{(2)}$	$\beta_{19}$	$i f \mathcal{H} \mu_3 G_2(\mathbf{k}_1, \mathbf{k}_2)/k_3$	$b_e - 2\mathcal{Q} - \mathcal{R}$

Here the  $\mathcal{C}$  functions in the Fourier kernels are

$$\mathcal{C}_1 = 2f - f^2 - 3\Omega_m, \quad (\text{A.20})$$

$$\mathcal{C}_2 = 2f - 1 + (1 - f) \left[ 6\Omega_m + f(1 - 2f) - 2f \frac{\mathcal{H}'}{\mathcal{H}^2} \right], \quad (\text{A.21})$$

$$\mathcal{C}_3 = 2f \left( 2f - 1 + \frac{\mathcal{H}'}{\mathcal{H}^2} \right) + 2 \frac{f'}{\mathcal{H}}, \quad (\text{A.22})$$

the  $\mathcal{A}$  functions in the coefficients are

$$\begin{aligned}
\mathcal{A}_1 = & -3 + 2f \left( 2 - 2b_e + 4\mathcal{Q} + \frac{4(1 - \mathcal{Q})}{\chi \mathcal{H}} + \frac{2\mathcal{H}'}{\mathcal{H}^2} \right) - \frac{2f'}{\mathcal{H}} + b_e^2 + 6b_e - 8b_e \mathcal{Q} + 4\mathcal{Q} \\
& + 16\mathcal{Q}^2 - 16 \frac{\partial \mathcal{Q}}{\partial \ln L} - 8 \frac{\mathcal{Q}'}{\mathcal{H}} + \frac{b_e'}{\mathcal{H}} + \frac{2}{\chi^2 \mathcal{H}^2} \left( 1 - \mathcal{Q} + 2\mathcal{Q}^2 - 2 \frac{\partial \mathcal{Q}}{\partial \ln L} \right) \\
& - \frac{2}{\chi \mathcal{H}} \left[ 4 + 2b_e - 2b_e \mathcal{Q} - 4\mathcal{Q} + 8\mathcal{Q}^2 - \frac{3\mathcal{H}'}{\mathcal{H}^2} (1 - \mathcal{Q}) - 8 \frac{\partial \mathcal{Q}}{\partial \ln L} - 2 \frac{\mathcal{Q}'}{\mathcal{H}} \right] \\
& + \frac{\mathcal{H}'}{\mathcal{H}^2} \left( -8 - 2b_e + 8\mathcal{Q} + \frac{3\mathcal{H}'}{\mathcal{H}^2} \right) - \frac{\mathcal{H}''}{\mathcal{H}^3}, \quad (\text{A.23})
\end{aligned}$$

$$\mathcal{A}_2 = 2\mathcal{H} \left[ -\frac{15}{2} + f(3 - b_e) - \frac{3}{2}b_e - 2b_e \frac{(1 - \mathcal{Q})}{\chi\mathcal{H}} + \frac{b'_e}{\mathcal{H}} + b_e^2 - 4b_e\mathcal{Q} + 12\mathcal{Q} + \frac{6(1 - \mathcal{Q})}{\chi\mathcal{H}} - 2\left(2 - \frac{1}{\chi\mathcal{H}}\right) \frac{\mathcal{Q}'}{\mathcal{H}} \right], \quad (\text{A.24})$$

$$\mathcal{A}_3 = 2\mathcal{H} \left[ -3 + 4b_e + \frac{2b_e(1 - \mathcal{Q})}{\chi\mathcal{H}} - b_e^2 + 2b_e\mathcal{Q} - 6\mathcal{Q} - \frac{b'_e}{\mathcal{H}} - \frac{6(1 - \mathcal{Q})}{\chi\mathcal{H}} + 2\left(1 - \frac{1}{\chi\mathcal{H}}\right) \frac{\mathcal{Q}'}{\mathcal{H}} \right], \quad (\text{A.25})$$

$$\begin{aligned} \mathcal{A}_4 = & 4 + 2f \left[ -3 + f + 2b_e - 3\mathcal{Q} - \frac{4(1 - \mathcal{Q})}{\chi\mathcal{H}} - \frac{2\mathcal{H}'}{\mathcal{H}^2} \right] + \frac{2f'}{\mathcal{H}} - 6b_e - 2b_e^2 + 12b_e\mathcal{Q} - 8\mathcal{Q} \\ & - 16\mathcal{Q}^2 + 16 \frac{\partial\mathcal{Q}}{\partial\ln L} + 12 \frac{\mathcal{Q}'}{\mathcal{H}} - 2 \frac{b'_e}{\mathcal{H}} - \frac{4}{\chi^2\mathcal{H}^2} \left( 1 - \mathcal{Q} + 2\mathcal{Q}^2 - 2 \frac{\partial\mathcal{Q}}{\partial\ln L} \right) \\ & - \frac{4}{\chi\mathcal{H}} \left( -1 - 2b_e + 2b_e\mathcal{Q} + \mathcal{Q} - 6\mathcal{Q}^2 + \frac{3\mathcal{H}'}{\mathcal{H}^2} (1 - \mathcal{Q}) + 6 \frac{\partial\mathcal{Q}}{\partial\ln L} + 2 \frac{\mathcal{Q}'}{\mathcal{H}} \right) \\ & + \frac{2\mathcal{H}'}{\mathcal{H}^2} \left( 3 + 2b_e - 6\mathcal{Q} - \frac{3\mathcal{H}'}{\mathcal{H}^2} \right) + \frac{2\mathcal{H}''}{\mathcal{H}^3}, \end{aligned} \quad (\text{A.26})$$

$$\begin{aligned} \mathcal{A}_5 = & -4 - b_e + b_e^2 - 4b_e\mathcal{Q} + 6\mathcal{Q} + 4\mathcal{Q}^2 - 4 \frac{\partial\mathcal{Q}}{\partial\ln L} - 4 \frac{\mathcal{Q}'}{\mathcal{H}} + \frac{b'_e}{\mathcal{H}} \\ & + \frac{2}{\chi^2\mathcal{H}^2} \left( 1 - \mathcal{Q} + 2\mathcal{Q}^2 - 2 \frac{\partial\mathcal{Q}}{\partial\ln L} \right) \\ & + \frac{2}{\chi\mathcal{H}} \left[ 3 - 2b_e + 2b_e\mathcal{Q} - 3\mathcal{Q} - 4\mathcal{Q}^2 + \frac{3\mathcal{H}'}{\mathcal{H}^2} (1 - \mathcal{Q}) + 4 \frac{\partial\mathcal{Q}}{\partial\ln L} + 2 \frac{\mathcal{Q}'}{\mathcal{H}} \right] \\ & + \frac{\mathcal{H}'}{\mathcal{H}^2} \left( 3 - 2b_e + 4\mathcal{Q} + \frac{3\mathcal{H}'}{\mathcal{H}^2} \right) - \frac{\mathcal{H}''}{\mathcal{H}^3}, \end{aligned} \quad (\text{A.27})$$

and the functions  $\mathcal{R}, \mathcal{S}$  in the coefficients are

$$\mathcal{R} = \frac{2(1 - \mathcal{Q})}{\chi\mathcal{H}} + \frac{\mathcal{H}'}{\mathcal{H}^2}, \quad (\text{A.28})$$

$$\mathcal{S} = 4 \left( 2 - \frac{1}{\chi\mathcal{H}} \right) \frac{\partial b_{10}}{\partial\ln L}. \quad (\text{A.29})$$

The magnification bias is defined by [9, 12, 66]:

$$\mathcal{Q} = - \frac{\partial \ln \bar{n}_g}{\partial \ln L} \Big|_c, \quad (\text{A.30})$$

where  $L$  is the background luminosity and the derivative is evaluated at the flux cut. Similarly,  $\partial b_{10}/\partial \ln L$  is understood to be evaluated at the flux cut. We use a short-hand notation for the second luminosity derivative of  $\bar{n}_g$ :

$$\frac{\partial \mathcal{Q}}{\partial \ln L} \equiv - \frac{\partial^2 \ln \bar{n}_g}{\partial (\ln L)^2} \Big|_c. \quad (\text{A.31})$$

## B $\Upsilon_I$ functions in (3.26)

$$\begin{aligned} \frac{1}{f_{\text{NL}}} \frac{\Upsilon_1}{\mathcal{H}^2} &= 2(3 - b_e)f + 3\Omega_m \left[ 1 + b_e - 4\mathcal{Q} - \frac{2(1 - \mathcal{Q})}{\chi\mathcal{H}} - \frac{\mathcal{H}'}{\mathcal{H}^2} \right] \\ &\quad + \frac{6\Omega_m}{(3\Omega_m + 2f)} \left[ \frac{f'}{\mathcal{H}} + \left( 1 + 2\frac{\mathcal{H}'}{\mathcal{H}^2} \right) f \right] \end{aligned} \quad (\text{B.1})$$

$$\frac{1}{f_{\text{NL}}} \frac{\Upsilon_2}{\mathcal{H}} = 2f \left[ b_e - 2\mathcal{Q} - \frac{2(1 - \mathcal{Q})}{\chi\mathcal{H}} - \frac{\mathcal{H}'}{\mathcal{H}^2} \right] \quad (\text{B.2})$$

$$\begin{aligned} \frac{1}{b_{01}} \frac{\Upsilon_3}{\mathcal{H}^2} &= \frac{3}{2}\Omega_m \left[ 2 + b_e - 4\mathcal{Q} + \frac{2(1 - \mathcal{Q})}{\chi\mathcal{H}} + \frac{\mathcal{H}'}{\mathcal{H}^2} + 2 \left( 2 - \frac{1}{\chi\mathcal{H}} \right) \frac{\partial \ln b_{01}}{\partial \ln L} \right] \\ &\quad + f \left[ 3 - f - b_e + \frac{1}{2} \frac{\partial \ln b_{01}}{\partial \ln a} \right] \end{aligned} \quad (\text{B.3})$$

$$\frac{1}{b_{01}} \frac{\Upsilon_4}{\mathcal{H}} = -\frac{3}{2}\Omega_m \quad (\text{B.4})$$

$$\frac{1}{b_{01}} \frac{\Upsilon_5}{\mathcal{H}} = f \left[ f + b_e - 2\mathcal{Q} - \frac{2(1 - \mathcal{Q})}{\chi\mathcal{H}} - \frac{\mathcal{H}'}{\mathcal{H}^2} + 2 \left( 2 - \frac{1}{\chi\mathcal{H}} \right) \frac{\partial \ln b_{01}}{\partial \ln L} \right] \quad (\text{B.5})$$

Note that  $\Upsilon_2 = 2f_{\text{NL}} \gamma_1$ .

**Table 3.** The  $f_{\text{NL}} \neq 0$  terms from relativistic projection effects [see (3.26)].

TERM	$\Upsilon$	FOURIER KERNEL	COEFFICIENT
$V_{\text{nG}}^{(2)}$	$\Upsilon_1$	$2f_{\text{NL}} \mathcal{H} f \mathcal{M}_3 / (\mathcal{M}_1 \mathcal{M}_2 k_3^2)$	$(3 - b_e)\mathcal{H}$
$\Psi_{\text{nG}}^{(2)} = \Phi_{\text{nG}}^{(2)}$	$\Upsilon_1$	$-3f_{\text{NL}} \Omega_m \mathcal{H}^2 \mathcal{M}_3 / (\mathcal{M}_1 \mathcal{M}_2 k_3^2)$	$4\mathcal{Q} - 1 - b_e + \mathcal{R}$
$\Psi_{\text{nG}}^{(2)'} $	$\Upsilon_1$	$6f_{\text{NL}} [f' + (\mathcal{H} + 2\mathcal{H}'/\mathcal{H})f] \Omega_m \mathcal{H}^2 \mathcal{M}_3 / [(3\Omega_m + 2f)(\mathcal{M}_1 \mathcal{M}_2 k_3^2)]$	$1/\mathcal{H}$
$\partial_{\parallel} V_{\text{nG}}^{(2)}$	$\Upsilon_2$	$i 2f_{\text{NL}} \mathcal{H} f \mu_3 \mathcal{M}_3 / (\mathcal{M}_1 \mathcal{M}_2 k_3)$	$b_e - 2\mathcal{Q} - \mathcal{R}$
$\Psi \varphi_{\text{P}}$	$\Upsilon_3$	$-3\Omega_m \mathcal{H}^2 [(k_1^2/\mathcal{M}_1) + (k_2^2/\mathcal{M}_2)] / (4k_1^2 k_2^2)$	$b_{01} [8\mathcal{Q} + 2\mathcal{R} - 2b_e - 4 - \mathcal{S}/(b_{10} - 1)]$
$V \varphi_{\text{P}}$	$\Upsilon_3$	$f \mathcal{H} [(k_1^2/\mathcal{M}_1) + (k_2^2/\mathcal{M}_2)] / (2k_1^2 k_2^2)$	$b_{01} [2(3 - b_e - f)\mathcal{H} + b'_{10}/(b_{10} - 1)]$
$\Psi \partial_{\parallel} \varphi_{\text{P}}$	$\Upsilon_4$	$-i 3\Omega_m \mathcal{H}^2 [(\mu_1 k_1^3/\mathcal{M}_1) + (\mu_2 k_2^3/\mathcal{M}_2)] / (4k_1^2 k_2^2)$	$2b_{01}/\mathcal{H}$
$\varphi_{\text{P}} \partial_{\parallel} V$	$\Upsilon_5$	$i f \mathcal{H} [(\mu_1 k_2/\mathcal{M}_2) + (\mu_2 k_1/\mathcal{M}_1)] / (2k_1 k_2)$	$b_{01} [2f + 2b_e - 4\mathcal{Q} - 2\mathcal{R} + \mathcal{S}/(b_{10} - 1)]$

## References

- [1] W. L. W. Sargent and E. L. Turner, *A statistical method for determining the cosmological density parameter from the redshifts of a complete sample of galaxies*, *Astrophys. J.* **212** (1977) L3–L7.
- [2] N. Kaiser, *Clustering in real space and in redshift space*, *Mon. Not. Roy. Astron. Soc.* **227** (1987) 1–27.
- [3] J. V. Villumsen, *Clustering of faint galaxies:  $\omega(\theta)$  induced by weak gravitational lensing*, [astro-ph/9512001](#).
- [4] J. Yoo, A. Fitzpatrick, and M. Zaldarriaga, *A New Perspective on Galaxy Clustering as a Cosmological Probe: General Relativistic Effects*, *Phys. Rev. D* **80** (2009) 083514, [[arXiv:0907.0707](#)].
- [5] J. Yoo, *General Relativistic Description of the Observed Galaxy Power Spectrum: Do We Understand What We Measure?*, *Phys. Rev.* **D82** (2010) 083508, [[arXiv:1009.3021](#)].
- [6] A. Challinor and A. Lewis, *The linear power spectrum of observed source number counts*, *Phys. Rev.* **D84** (2011) 043516, [[arXiv:1105.5292](#)].
- [7] C. Bonvin and R. Durrer, *What galaxy surveys really measure*, *Phys. Rev.* **D84** (2011) 063505, [[arXiv:1105.5280](#)].
- [8] A. Hall, C. Bonvin, and A. Challinor, *Testing General Relativity with 21-cm intensity mapping*, *Phys. Rev. D* **87** (2013), no. 6 064026, [[arXiv:1212.0728](#)].
- [9] D. Alonso, P. Bull, P. G. Ferreira, R. Maartens, and M. Santos, *Ultra large-scale cosmology in next-generation experiments with single tracers*, *Astrophys. J.* **814** (2015), no. 2 145, [[arXiv:1505.07596](#)].
- [10] J. Fonseca, S. Camera, M. Santos, and R. Maartens, *Hunting down horizon-scale effects with multi-wavelength surveys*, *Astrophys. J. Lett.* **812** (2015), no. 2 L22, [[arXiv:1507.04605](#)].
- [11] O. Umeh, R. Maartens, and M. Santos, *Nonlinear modulation of the HI power spectrum on ultra-large scales. I*, *JCAP* **1603** (2016), no. 03 061, [[arXiv:1509.03786](#)].
- [12] E. Di Dio, R. Durrer, G. Marozzi, and F. Montanari, *The bispectrum of relativistic galaxy number counts*, *JCAP* **01** (2016) 016, [[arXiv:1510.04202](#)].
- [13] S. Jolicoeur, R. Maartens, E. M. De Weerd, O. Umeh, C. Clarkson, and S. Camera, *Detecting the relativistic bispectrum in 21cm intensity maps*, [arXiv:2009.06197](#).
- [14] M. Bruni, R. Crittenden, K. Koyama, R. Maartens, C. Pitrou, and D. Wands, *Disentangling non-Gaussianity, bias and GR effects in the galaxy distribution*, *Phys. Rev.* **D85** (2012) 041301, [[arXiv:1106.3999](#)].
- [15] D. Jeong, F. Schmidt, and C. M. Hirata, *Large-scale clustering of galaxies in general relativity*, *Phys. Rev.* **D85** (2012) 023504, [[arXiv:1107.5427](#)].
- [16] N. Dalal, O. Dore, D. Huterer, and A. Shirokov, *The imprints of primordial non-gaussianities on large-scale structure: scale dependent bias and abundance of virialized objects*, *Phys. Rev.* **D77** (2008) 123514, [[arXiv:0710.4560](#)].
- [17] S. Matarrese and L. Verde, *The effect of primordial non-Gaussianity on halo bias*, *Astrophys. J. Lett.* **677** (2008) L77–L80, [[arXiv:0801.4826](#)].
- [18] T. Baldauf, U. Seljak, and L. Senatore, *Primordial non-Gaussianity in the Bispectrum of the Halo Density Field*, *JCAP* **1104** (2011) 006, [[arXiv:1011.1513](#)].
- [19] V. Desjacques, D. Jeong, and F. Schmidt, *Large-Scale Galaxy Bias*, *Phys. Rept.* **733** (2018) 1–193, [[arXiv:1611.09787](#)].

- [20] E. Villa and C. Rampf, *Relativistic perturbations in  $\Lambda$ CDM: Eulerian & Lagrangian approaches*, *JCAP* **1601** (2016), no. 01 030, [[arXiv:1505.04782](#)].
- [21] S. Camera, R. Maartens, and M. G. Santos, *Einstein’s legacy in galaxy surveys*, *Mon. Not. Roy. Astron. Soc.* **451** (2015), no. 1 L80–L84, [[arXiv:1412.4781](#)].
- [22] L. Lopez-Honorez, O. Mena, and S. Rigolin, *Biases on cosmological parameters by general relativity effects*, *Phys. Rev. D* **85** (2012) 023511, [[arXiv:1109.5117](#)].
- [23] J. Yoo, N. Hamaus, U. Seljak, and M. Zaldarriaga, *Going beyond the Kaiser redshift-space distortion formula: a full general relativistic account of the effects and their detectability in galaxy clustering*, *Phys. Rev. D* **86** (2012) 063514, [[arXiv:1206.5809](#)].
- [24] A. Raccañelli, D. Bertacca, O. Doré, and R. Maartens, *Large-scale 3D galaxy correlation function and non-Gaussianity*, *JCAP* **08** (2014) 022, [[arXiv:1306.6646](#)].
- [25] S. Camera, M. G. Santos, and R. Maartens, *Probing primordial non-Gaussianity with SKA galaxy redshift surveys: a fully relativistic analysis*, *Mon. Not. Roy. Astron. Soc.* **448** (2015), no. 2 1035–1043, [[arXiv:1409.8286](#)].
- [26] A. Raccañelli, F. Montanari, D. Bertacca, O. Doré, and R. Durrer, *Cosmological Measurements with General Relativistic Galaxy Correlations*, *JCAP* **05** (2016) 009, [[arXiv:1505.06179](#)].
- [27] D. Alonso and P. G. Ferreira, *Constraining ultralarge-scale cosmology with multiple tracers in optical and radio surveys*, *Phys. Rev. D* **92** (2015), no. 6 063525, [[arXiv:1507.03550](#)].
- [28] J. Fonseca, R. Maartens, and M. G. Santos, *Probing the primordial Universe with MeerKAT and DES*, *Mon. Not. Roy. Astron. Soc.* **466** (2017), no. 3 2780–2786, [[arXiv:1611.01322](#)].
- [29] L. R. Abramo and D. Bertacca, *Disentangling the effects of Doppler velocity and primordial non-Gaussianity in galaxy power spectra*, *Phys. Rev. D* **96** (2017), no. 12 123535, [[arXiv:1706.01834](#)].
- [30] C. S. Lorenz, D. Alonso, and P. G. Ferreira, *Impact of relativistic effects on cosmological parameter estimation*, *Phys. Rev. D* **97** (2018), no. 2 023537, [[arXiv:1710.02477](#)].
- [31] J. Fonseca, R. Maartens, and M. G. Santos, *Synergies between intensity maps of hydrogen lines*, *Mon. Not. Roy. Astron. Soc.* **479** (2018), no. 3 3490–3497, [[arXiv:1803.07077](#)].
- [32] M. Ballardini, W. L. Matthewson, and R. Maartens, *Constraining primordial non-Gaussianity using two galaxy surveys and CMB lensing*, *Mon. Not. Roy. Astron. Soc.* **489** (2019), no. 2 1950–1956, [[arXiv:1906.04730](#)].
- [33] N. Grimm, F. Scaccabarozzi, J. Yoo, S. G. Biern, and J.-O. Gong, *Galaxy Power Spectrum in General Relativity*, [[arXiv:2005.06484](#)].
- [34] J. L. Bernal, N. Bellomo, A. Raccañelli, and L. Verde, *Beware of commonly used approximations II: estimating systematic biases in the best-fit parameters*, [[arXiv:2005.09666](#)].
- [35] M. S. Wang, F. Beutler, and D. Bacon, *Impact of Relativistic Effects on the Primordial Non-Gaussianity Signature in the Large-Scale Clustering of Quasars*, [[arXiv:2007.01802](#)].
- [36] M. Tellarini, A. J. Ross, G. Tasinato, and D. Wands, *Galaxy bispectrum, primordial non-Gaussianity and redshift space distortions*, *JCAP* **1606** (2016), no. 06 014, [[arXiv:1603.06814](#)].
- [37] D. Bertacca, R. Maartens, and C. Clarkson, *Observed galaxy number counts on the lightcone up to second order: I. Main result*, *JCAP* **1409** (2014), no. 09 037, [[arXiv:1405.4403](#)].
- [38] D. Bertacca, R. Maartens, and C. Clarkson, *Observed galaxy number counts on the lightcone up to second order: II. Derivation*, *JCAP* **1411** (2014), no. 11 013, [[arXiv:1406.0319](#)].
- [39] J. Yoo and M. Zaldarriaga, *Beyond the Linear-Order Relativistic Effect in Galaxy Clustering: Second-Order Gauge-Invariant Formalism*, *Phys. Rev. D* **90** (2014), no. 2 023513, [[arXiv:1406.4140](#)].

- [40] E. Di Dio, R. Durrer, G. Marozzi, and F. Montanari, *Galaxy number counts to second order and their bispectrum*, *JCAP* **12** (2014) 017, [[arXiv:1407.0376](#)]. [Erratum: *JCAP* **06**, E01 (2015)].
- [41] D. Bertacca, *Observed galaxy number counts on the light cone up to second order: III. Magnification bias*, *Class. Quant. Grav.* **32** (2015), no. 19 195011, [[arXiv:1409.2024](#)].
- [42] O. Umeh, K. Koyama, R. Maartens, F. Schmidt, and C. Clarkson, *General relativistic effects in the galaxy bias at second order*, *JCAP* **05** (2019) 020, [[arXiv:1901.07460](#)].
- [43] O. Umeh and K. Koyama, *The galaxy bias at second order in general relativity with Non-Gaussian initial conditions*, *JCAP* **12** (2019) 048, [[arXiv:1907.08094](#)].
- [44] A. Kehagias, A. Moradinezhad Dizgah, J. Noreña, H. Perrier, and A. Riotto, *A Consistency Relation for the Observed Galaxy Bispectrum and the Local non-Gaussianity from Relativistic Corrections*, *JCAP* **08** (2015) 018, [[arXiv:1503.04467](#)].
- [45] O. Umeh, S. Jolicoeur, R. Maartens, and C. Clarkson, *A general relativistic signature in the galaxy bispectrum: the local effects of observing on the lightcone*, *JCAP* **1703** (2017) 003, [[arXiv:1610.03351](#)].
- [46] S. Jolicoeur, O. Umeh, R. Maartens, and C. Clarkson, *Imprints of local lightcone projection effects on the galaxy bispectrum. II*, *JCAP* **1709** (2017) 040, [[arXiv:1703.09630](#)].
- [47] K. Koyama, O. Umeh, R. Maartens, and D. Bertacca, *The observed galaxy bispectrum from single-field inflation in the squeezed limit*, *JCAP* **07** (2018) 050, [[arXiv:1805.09189](#)].
- [48] L. Verde, L.-M. Wang, A. Heavens, and M. Kamionkowski, *Large scale structure, the cosmic microwave background, and primordial non-gaussianity*, *Mon. Not. Roy. Astron. Soc.* **313** (2000) L141–L147, [[astro-ph/9906301](#)].
- [49] R. Scoccimarro, E. Sefusatti, and M. Zaldarriaga, *Probing primordial non-Gaussianity with large-scale structure*, *Phys. Rev.* **D69** (2004) 103513, [[astro-ph/0312286](#)].
- [50] E. Sefusatti, M. Crocce, S. Pueblas, and R. Scoccimarro, *Cosmology and the Bispectrum*, *Phys. Rev. D* **74** (2006) 023522, [[astro-ph/0604505](#)].
- [51] E. Sefusatti and E. Komatsu, *The Bispectrum of Galaxies from High-Redshift Galaxy Surveys: Primordial Non-Gaussianity and Non-Linear Galaxy Bias*, *Phys. Rev. D* **76** (2007) 083004, [[arXiv:0705.0343](#)].
- [52] T. Giannantonio and C. Porciani, *Structure formation from non-Gaussian initial conditions: Multivariate biasing, statistics, and comparison with N-body simulations*, *Phys. Rev. D* **81** (2010), no. 6 063530, [[arXiv:0911.0017](#)].
- [53] M. Tellarini, A. J. Ross, G. Tasinato, and D. Wands, *Non-local bias in the halo bispectrum with primordial non-Gaussianity*, *JCAP* **1507** (2015), no. 07 004, [[arXiv:1504.00324](#)].
- [54] C. A. Watkinson, S. Majumdar, J. R. Pritchard, and R. Mondal, *A fast estimator for the bispectrum and beyond – a practical method for measuring non-Gaussianity in 21-cm maps*, *Mon. Not. Roy. Astron. Soc.* **472** (2017), no. 2 2436–2446, [[arXiv:1705.06284](#)].
- [55] S. Majumdar, J. R. Pritchard, R. Mondal, C. A. Watkinson, S. Bharadwaj, and G. Mellema, *Quantifying the non-Gaussianity in the EoR 21-cm signal through bispectrum*, *Mon. Not. Roy. Astron. Soc.* **476** (2018), no. 3 4007–4024, [[arXiv:1708.08458](#)].
- [56] D. Karagiannis, A. Lazanu, M. Liguori, A. Raccanelli, N. Bartolo, and L. Verde, *Constraining primordial non-Gaussianity with bispectrum and power spectrum from upcoming optical and radio surveys*, *Mon. Not. Roy. Astron. Soc.* **478** (2018), no. 1 1341–1376, [[arXiv:1801.09280](#)].
- [57] V. Yankelevich and C. Porciani, *Cosmological information in the redshift-space bispectrum*, *Mon. Not. Roy. Astron. Soc.* **483** (2019), no. 2 2078–2099, [[arXiv:1807.07076](#)].

- [58] D. Sarkar, S. Majumdar, and S. Bharadwaj, *Modelling the post-reionization neutral hydrogen (HI) 21-cm bispectrum*, *Mon. Not. Roy. Astron. Soc.* **490** (2019), no. 2 2880–2889, [[arXiv:1907.01819](#)].
- [59] D. Karagiannis, A. z. Slosar, and M. Liguori, *Forecasts on Primordial non-Gaussianity from 21 cm Intensity Mapping experiments*, [arXiv:1911.03964](#).
- [60] S. Bharadwaj, A. Mazumdar, and D. Sarkar, *Quantifying the Redshift Space Distortion of the Bispectrum I: Primordial Non-Gaussianity*, *Mon. Not. Roy. Astron. Soc.* **493** (2020), no. 1 594–602, [[arXiv:2001.10243](#)].
- [61] D. Karagiannis, J. Fonseca, R. Maartens, and S. Camera, *Probing primordial non-Gaussianity with the bispectrum of future 21cm intensity maps*, [arXiv:2010.07034](#).
- [62] A. Moradinezhad Dizgah, M. Biagetti, E. Sefusatti, V. Desjacques, and J. Noreña, *Primordial Non-Gaussianity from Biased Tracers: Likelihood Analysis of Real-Space Power Spectrum and Bispectrum*, [arXiv:2010.14523](#).
- [63] S. Jolicoeur, O. Umeh, R. Maartens, and C. Clarkson, *Imprints of local lightcone projection effects on the galaxy bispectrum. Part III. Relativistic corrections from nonlinear dynamical evolution on large-scales*, *JCAP* **1803** (2018), no. 03 036, [[arXiv:1711.01812](#)].
- [64] S. Jolicoeur, A. Allahyari, C. Clarkson, J. Larena, O. Umeh, and R. Maartens, *Imprints of local lightcone projection effects on the galaxy bispectrum IV: Second-order vector and tensor contributions*, *JCAP* **03** (2019) 004, [[arXiv:1811.05458](#)].
- [65] C. Clarkson, E. M. de Weerd, S. Jolicoeur, R. Maartens, and O. Umeh, *The dipole of the galaxy bispectrum*, *Mon. Not. Roy. Astron. Soc.* **486** (2019), no. 1 L101–L104, [[arXiv:1812.09512](#)].
- [66] R. Maartens, S. Jolicoeur, O. Umeh, E. M. De Weerd, C. Clarkson, and S. Camera, *Detecting the relativistic galaxy bispectrum*, *JCAP* **03** (2020) 065, [[arXiv:1911.02398](#)].
- [67] E. M. de Weerd, C. Clarkson, S. Jolicoeur, R. Maartens, and O. Umeh, *Multipoles of the relativistic galaxy bispectrum*, *JCAP* **05** (2020) 018, [[arXiv:1912.11016](#)].
- [68] O. Umeh, K. Koyama, and R. Crittenden, *Testing the equivalence principle on cosmological scales using the odd multipoles of galaxy cross-power spectrum and bispectrum*, [arXiv:2011.05876](#).
- [69] **Planck** Collaboration, N. Aghanim et al., *Planck 2018 results. VI. Cosmological parameters*, [arXiv:1807.06209](#).
- [70] T. Tram, C. Fidler, R. Crittenden, K. Koyama, G. W. Pettinari, and D. Wands, *The Intrinsic Matter Bispectrum in  $\Lambda$ CDM*, *JCAP* **1605** (2016), no. 05 058, [[arXiv:1602.05933](#)].
- [71] N. Bartolo, D. Bertacca, M. Bruni, K. Koyama, R. Maartens, S. Matarrese, M. Sasaki, L. Verde, and D. Wands, *A relativistic signature in large-scale structure*, *Phys. Dark Univ.* **13** (2016) 30–34, [[arXiv:1506.00915](#)].
- [72] D. Bertacca, N. Bartolo, M. Bruni, K. Koyama, R. Maartens, S. Matarrese, M. Sasaki, and D. Wands, *Galaxy bias and gauges at second order in General Relativity*, *Class. Quant. Grav.* **32** (2015), no. 17 175019, [[arXiv:1501.03163](#)].
- [73] L. Dai, E. Pajer, and F. Schmidt, *On Separate Universes*, *JCAP* **1510** (2015), no. 10 059, [[arXiv:1504.00351](#)].
- [74] R. de Putter, O. Doré, and D. Green, *Is There Scale-Dependent Bias in Single-Field Inflation?*, *JCAP* **1510** (2015), no. 10 024, [[arXiv:1504.05935](#)].
- [75] S. Matarrese, L. Pilo, and R. Rollo, *Resilience of long modes in cosmological observables*, [arXiv:2007.08877](#).

- [76] M. Bruni, J. C. Hidalgo, N. Meures, and D. Wands, *Non-Gaussian Initial Conditions in  $\Lambda$ CDM: Newtonian, Relativistic, and Primordial Contributions*, *Astrophys. J.* **785** (2014) 2, [[arXiv:1307.1478](#)].
- [77] P. Gagrani and L. Samushia, *Information Content of the Angular Multipoles of Redshift-Space Galaxy Bispectrum*, *Mon. Not. Roy. Astron. Soc.* **467** (2017), no. 1 928–935, [[arXiv:1610.03488](#)].